NSG-1242

NUMERICAL SOLUTION OF THE NAVIER-STOKES EQUATIONS FOR SUPER-SONIC FLOWS WITH STRONG SHOCKS

By

Krishna Devarayalu

A Dissertation
Submitted to the Faculty of
Mississippi State University
in Partial Fulfillment of the Requirements
for the Degree of Doctor of Philosophy
in the College of Engineering

Mississippi State, Mississippi

August 1978

NUMERICAL SOLUTION OF THE NAVIER-STOKES EQUATIONS

FOR SUPER-SONIC FLOWS WITH STRONG SHOCKS

By

Krishna Devarayalu

A Dissertation
Submitted to the Faculty of
Mississippi State University
in Partial Fulfillment of the Requirements
for the Degree of Doctor of Philosophy
in the College of Engineering

Mississippi State, Mississippi

August 1978

NUMERICAL SOLUTION OF THE NAVIER-STOKES EQUATIONS

FOR SUPER-SONIC FLOWS WITH STRONG SHOCKS

By

Krishna Devarayalu

Associate Professor of Aerophysics and Aerospace Engineering (Director of Dissertation and Chairman of Advisory Committee)

Professor of Aerophysics and Aerospace Engineering (Member of Committee)

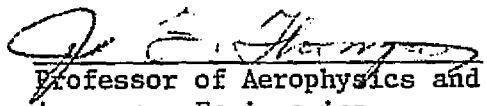

Professor of Aerophysics and Aerospace Engineering (Member of Committee)

Professor of Aerophysics and Aerospace Engineering (Member of Committee)

Professor and Head of the Department of Mathematics (Member of Committee)

Professor and Head of the Department of Aerophysics and Aerospace Engineering

Dean of the College of Engineering

Dean of the Graduate School

August, 1978

ACKNOWLEDGEMENT

First and foremost, I must express my sincere appreciation to Prof. Z. U. A. Warsi, who, as my major professor, bore the brunt of the task of supervision. His knowledge, dedication, and perseverance contributed in no small measure to the shaping up of my dissertation.

Prof. J. F. Thompson has been the guiding light and inspiration for this research. But for the innumerable computer programs and subroutines that were developed both by him as well as his former students, this work would have been well nigh impossible.

"No work is done until the paper work is finished," is Mrs. Nancie Upchurch's motto. She did an excellent job of typing the manuscript, particularly the long and contorted equations. Working long and patient hours, Annie Miley did complete the figures and the viewgraphs in time for my defense, as she always, optimistically, believed she would. Nancie and Annie certainly did make the task of putting together a dissertation a very pleasant experience.

Last but not least, I must express my gratitude to the graduate students, staff, and faculty of this department whose friendliness, informality, and helpfulness contributed to making the past four years of my stay here a happy one. This research was partially supported by NASA Grant NSG 1242.

K.D.

Mississippi State University

August, 1978

ABSTRACT

Krishna Devarayalu, Doctor of Philosophy, 1978

Major: Engineering, Department of Aerophysics and Aerospace Engineering

Title of Dissertation: Numerical Solution of the Navier-Stokes Equations for Super-Sonic Flows with Strong Shocks

Directed by: Dr. Z. U. A. Warsi

Pages in Dissertation: 86 Words in Abstract: 405

ABSTRACT

The numerical solution of the full Navier-Stokes Equations for viscous flows with high Mach numbers and a strong detached bow shock is obtained. Two dimensional flows around (a) a circular cylinder, and (b) a circular cylinder with an aft-body in the form of a fairing, have been considered. The solution of the compressible N.S. Equations was accomplished by the method of finite differences. An implicit scheme of solution, the S.O.R., was used with the optimum acceleration parameters determined by trial and error. The tensor notation was used in writing the N-S Equations transformed into general curvilinear coordinates. The coordinate system used is a general non-orthogonal curvilinear system with coordinate lines coincident with all boundaries. This coordinate system is numerically generated. The computational domain is limited upstream by a boundary located at a short distance ahead of the bow shock. The shock has been treated as a sharp but continuous transition zone. (Shock capturing method.) The boundary conditions at this upstream boundary are the uniform flow conditions. The Euler equations were solved on the exit plane to establish the

downstream boundary conditions. The capability of attracting the coordinate lines to other pre-designated lines and, or, points exists. This technique was applied to blunt body flows with strong-shock to concentrate in and define the region of the shock. The amount of concentration was controlled by the factors "attraction amplitude" and "exponential decay" which were expressed as functions of the local density gradient across the shock. The equations for the generation of the coordinate system (using coordinate control) were solved, followed by the solution of the N.S. Equations, at the end of a set of given number of time steps. This process was repeated for different sets; thus the coordinate system concentrated in the shock region and moved with the shock. "Wiggles", by far constituted the one major problem that needed to be overcome. These oscillations that were encountered had no physical meaning and gave rise to quantities such as negative temperatures, which ultimately caused the computational program to break down. It was found that the application of certain dissipative finite-difference schemes damped these oscillations. The Shuman Filter, in particular, proved the most effective. The results are obtained for a Mach No. of 4.6 and a Reynolds No. of 10,000, and are compared with the experimental results available for these free stream conditions of flow around a circular cylinder.

TABLE OF CONTENTS

LIST OF SYMBOLS

a = Local Speed of Sound

A = σu (Dependent Variable)

A_k = Amplitude Factor for η-Line Attraction

A'_k = Amplitude Factor for ξ-Line Attraction

B = σv (Dependent Variable)

B_ℓ = Amplitude Factor for η-Point Attraction

B'_ℓ = Amplitude Factor for ξ-Point Attraction

c_p^* = Specific Heat at Constant Pressure (Dimensional)

C_p = Pressure Coefficient

$\tilde{d}$ = Deformation Tensor

D_k = Decay Factor for η-Line Attraction

D'_k = Decay Factor for ξ-Line Attraction

D^{ij} = $\sqrt{g}\, d^{ij}$, $i = 1,2$, $j = 1,2$

e = Non-dimensional Specific Internal Energy

E = $\sqrt{g}\,\Psi$ (Dependent Variable)

E_ℓ = Decay Factor for η-Point Attraction

E'_ℓ = Decay Factor for ξ-Point Attraction

f = Scalar Function (Surrogate)

g = Det (g_{ij})

g_{ij} = Covariant Components of the Metric Tensor

g^{ij} = Contravariant Components of the Metric Tensor

G_{ij} = $g_{ij}/\sqrt{g}$

H = $\sigma(u)^2$

$i,j,\ldots$ = Subscripts in Index Notation

$\tilde{I}$ = Idem Tensor; Equal to δ_{ij} when Referred to Cartesian Coordinates and g_{ij} or g^{ij} when Referred to Curvilinear Coordinates

I,J = Integers

IMAX, JMAX = Maximum Values of I and J Used

I_{B1}, I_{B2} = Values of I where the Cut Meets the Body

I_{UC}, I_{LC} = Integers Representing I Values on the Upper and Lower Parts of the Cut Respectively, Fig. 5

J = Jacobian where Stated

k^* = Conductivity (Dimensional)

K = λ div $\underline{v}$

K_n = Knudsen Number

m,m' = Number of Points Involved in Attraction Along the ξ-Direction

M = $\sigma(v)^2$

M_ℓ = Local Mach Number

M_∞ = Free Stream Mach Number

$\underline{n}$ = Unit Normal Vector

n,n' = Number of η-Lines Involved in η-Line Attraction

N = σuv

p = Nondimensional Pressure

P = $\sqrt{g}\ p$

P_r = Prandtl Number

Q = (E+P)u

R = (E+P)v

R_e = $\dfrac{2\rho^*_\infty V^*_\infty R^*_n}{\mu^*_\infty}$, Free Stream Reynolds Number

R^*_n = Nose Radius (Dimensional)

S_1 = Sutherland's Constant

sgn = Sign Function

$\underset{\sim}{t}$ = Unit Tangent Vector

T = T^*/T^*_∞ , Nondimensional Temperature

u = v^1, Contravariant Velocity Component

v = v^2, Contravariant Velocity Component

U,V = Cartesian Velocity Components

v^i = Contravariant Components

v_i = Covariant Components

$\underset{\sim}{v}$ = $\underset{\sim}{v}^*/V^*_\infty$, Nondimensional Velocity Vector

$v^i_{,j}$ = Covariant Derivative

(x,y) = Nondimensional Cartesian Coordinates

x_ℓ = Cartesian Coordinates ($x_1 = x$, $x_2 = y$)

α_o = Nondimensional Constant, Eq. (3.4)

Γ^i_{jk} = Christoffel Symbols

γ = c^*_p/c^*_v, Adiabatic Exponent

ξ,η = Transformed Coordinate System

ξ^i = General Curvilinear Coordinate System, ($\xi^1 = \xi$, $\xi^2 = \eta$)

ξ_k, η_k = Values of ξ and η for Varying k, Eq. (2.11)

Ψ = Total Energy

ρ = ρ^*/ρ^*_∞, Nondimensional Density

σ = $\sqrt{g}\,\rho$ (Dependent Variable)

$\tilde{\sigma}$ = Stress Tensor

μ = μ^*/μ^*_∞, Nondimensional Viscosity

λ = λ^*/μ^*_∞, Nondimensional Bulk Viscosity; also a Surrogate Variable where Stated

$\tilde{\tau}$ = Tensor

ϵ = $1/R_e$

ω = Vorticity; also as Acceleration Parameter where Stated

δ_{ij} = Kronecker-δ

Operators:

div = Divergence

grad = Gradient

$(\ )^T$ = Transpose

Subscripts:

$\sim$ = Denotes Vector

ξ, η = Partial Differentiation

∞ = Free Stream Value

w = Wall Value

ij = Covariant Tensor

,j = Covariant Derivative

i = Covariant Vector; when used with x or ξ, then no Tensorial Significance

s = Stagnation Value

Superscripts:

$\sim$ = Denotes a Tensor

* = Denotes a Dimensional Quantity

ij = Contravariant Tensor

i = Contravariant Vector

LIST OF FIGURES

CHAPTER I

INTRODUCTION

In the accurate numerical prediction of real flows in general, there remain serious difficulties due to the complexity of these flows arising from unsteadiness, turbulence, three-dimensional character, large variations of flow gradients, etc. The numerical solution of the full equations for viscous flows, i.e., the Navier-Stokes Equations has, thus, attracted much attention, to treat fluid flow problems for which no simplified model exists. Generally it is found that the N-S Equations apply when the continuum hypothesis is satisfied; this condition being satisfied when the Knudsen Number is less than 0.01. Victoria and Widhopf [1] reported that the use of the N-S Equations to solve hypersonic low Reynolds/high Knudsen Number flow problems, is valid. They considered the flow about a sphere in a Mach 10 flow at a free stream Reynolds Number of 152, with a corresponding Knudsen Number of 0.10. The range of validity of the N-S Equations does, indeed, seem to cover most of the aerodynamic problems relating to aeronautics and astronautics.

The present investigation concerns the numerical solution of the complete N-S Equations for viscous flows, with strong shocks, ahead of a two-dimensional arbitrary body. The detached bow shock separates the flow disturbed by the body from the undistrubed flow. Behind the shock wave there is a sub-sonic region bounded by it, the body and the "sonic lines." The flow field outside of this sub-sonic region is again super-sonic, with the exception of the region of the wake immediately behind the body. The shape of the bow shock ahead of the body is

influenced by the shape of its leading edge. The numerical solution of the compressible N-S Equations in the case of a mixed sub-sonic and super-sonic flow field as described above is a difficult task and cannot yet be ranked along with the standard theoretical tools currently used in applied aerodynamics.

Of the various types of methods in use for the numerical solution of the N-S Equations, the finite-difference method is perhaps, by far the most widely used. In the last few years, finite-element methods have received increasing attention as a substitute to finite-difference methods in fluid mechanics problems, particularly in the solution of the incompressible N-S Equations.

To keep the computing time within reasonable bounds it is important to minimize the number of mesh points and this usually requires that the mesh system be taken non-uniform in the physical plane. This can be achieved by imposing a variable mesh spacing in a given coordinate system. The mesh system is generally also chosen so as to make the boundaries of the computational domain, particularly solid walls, coincide with mesh lines; this considerably simplifies the treatment of boundary conditions. One of the novel features of the present research is the use of the body fitted coordinates which are a system of general curvilinear coordinates, that are numerically generated, developed by Thompson, et. al., [2] and Thames [3]. This system of coordinate generation is quite versatile due to the fact that it allows the coordinate lines to be coincident with all boundaries of a general multiply connected region including the boundaries formed by the solid walls of any number of quite arbitrarily shaped bodies. The boundaries may even be time-dependent. Thus with this procedure the numerical

solution of the N-S Equations may be obtained on a fixed rectangular field or the transformed plane, with a square mesh. No interpolation of the flow variables is required regardless of the shape of the physical boundaries or the spacing of the curvilinear coordinate lines in the physical plane.

Once the coordinate system has been chosen, and the choice of a mesh size is made, various techniques may be made use of to reduce the computing time as much as possible for a given numerical scheme. In an explicit scheme of solution, the local maximum time step depends strongly on the local mesh size in physical space; if the physical mesh varies considerably throughout the computational domain, the time step will be determined by the smallest mesh and will be, in all probability, very small. It is then practically indispensable to divide the domain into several regions in each of which a different time step is used so as to reduce the total number of operations necessary to advance the solution in time in the entire field - all of which leads to computational complications and restrictions. Thus it is seen that time step limitation is the main drawback of explicit schemes; however, these methods have been widely used because of their simplicity and the fact that the number of numerical operations at each step is kept to a minimum. Another approach which is attracting more attention now is the use of implicit schemes which lead to less severe stability conditions or which are unconditionally stable. Roger Peyret and Henri Viviand [4] concluded (in 1975) that "no clear cut conclusion can be drawn at this time regarding the best type of method - implicit or explicit." However, the fact that an implicit scheme is unconditionally stable proved irresistable and one such scheme - the S.O.R. -

was used in the present work. Also tensor notation was used in writing the N-S Equations transformed into general curvilinear coordinates as this measure greatly simplified the overall problem of analytical development and rendered the method more general. Thus the extension of the method to three dimensions is now purely formal.

The flow considered being super-sonic about a blunt body, a detached bow shock exists ahead of the body, as noted earlier. The computational domain was limited upstream by a boundary located at a short distance ahead of the bow shock, treating the shock as a thin but continuous transition zone. This is the "shock capturing" method. Tannehill and Holst [5] used this approach for low Reynolds Number flows. However, they found that (as indeed, we too) for high Reynolds Number flows it was not "practical" to capture the bow shock because of the numerical difficulties associated with the large gradients at the bow shock. Instead, they found it more convenient to treat the bow shock as a discontinuity, across which the Rankine-Hugoniot Equations could be applied, while leaving the boundary layer to be "captured." This approach is called the "shock-fitting" method and is generally favored because, the flow being practically inviscid in the vicinity of the shock, the N-S Equations are not really needed to calculate the shock; but the problems associated with this method are those that arise due to the necessity of having to couple the inviscid and viscous flow solutions and the a priori definition of inviscid and viscous regions. The shock-capturing method was used in this research, not withstanding the numerical difficulties associated with this method, because it is much more convenient to solve the N-S Equations in the entire flow field when the inviscid flow region is of a small extent. This situation

exists in the case of bow shocks in high Mach number flows. Now the thickness δ_s of a normal shock wave in real viscous fluids varies as 1/Re for fixed Pr. For high Reynolds Number flows it then becomes likely that $\delta_s < \Delta x$ (the mesh size normal to the shock). When this occurs, oscillations develop aft of the shock leading to the numerical difficulties as reported by Tannehill and Holst and a host of other investigators. If $1/Re \to 0$ and if the finite-difference method has no artificial viscosity, then there is no dissipative mechanism by which the oscillations may be damped out. Many authors have associated these spatial oscillations, also called "wiggles," with non-linearities, or with linear instabilities in the transient calculation. Roache [6] has however, demonstrated that wiggles are not caused by iterative instability or non-linearities, but that they simply are a solution of the finite-difference equation used. In the numerical computation of flow fields containing shock waves, these oscillations or wiggles may be damped by the application of dissipative finite-difference schemes. The concept of introducing an implicit dissipation term by using a dissipative finite-difference scheme to damp out short wave oscillations has been used by many researchers. Vliegenthart [7] reported that these encountered oscillations which have no physical meaning, can be suppressed by applying Shuman's technique of introducing dissipation, and that, in certain cases this even appears to remove nonlinear instabilities as in the case of the computation of a detached shock in front of a blunt-body. Due to its extreme simplicity and effectiveness the Shuman Filter, which is discussed in Chapter IV, has been used in the present research, to overcome the problem of wiggles. Unlike other schemes, the Lax-Wendroff, for instance, the

Shumann Filter is not an integral part of the difference approximation. Lax's scheme, yields a shock which is spread out over a large number of mesh spacings, while the Shumann Filter yields a shock which is considerably narrower.

The capability of attracting the coordinate lines to other pre-designated coordinate lines or grid points exists at present, and through the application of this technique to blunt body flows with strong shocks, an effort was made to concentrate in, and define, the region of the shock. The magnitude of concentration is controlled by the factors "attraction amplitude" and "exponential decay." (These terms are discussed in Chapter II.) These cooordinate control factors were expressed as functions of the local density gradient across the shock. The equations for the generation of the coordinate system, using coordinate control, were solved, followed by the solution of the N-S Equations, at the end of a set of given number of time steps. This process was repeated for different sets of time steps. Thus the coordinate system was refined in the region of the shock and moved with the shock. This measure obviated the need of having a very refined mesh in the entire computational domain by providing refinement only in the region through which the shock happened to be passing at any given time.

The results presented pertain to a flow about a two-dimensional circular cylinder with a free stream Mach Number of 4.6 and a Reynolds Number of 10^4. A few results for the case of a circular cylinder with an aft body (fairing) have also been included for comparisons. The wall pressure, normalized with respect to the stagnation pressure, as

reported by Tannehill and Holst [5] has been compared with the present solution for the circular cylinder and the two results are in good agreement. All the numerical results are discussed in Chapter v.

CHAPTER II

NUMERICAL GENERATION OF CURVILINEAR COORDINATES

2.1. The Boundary-Fitted Coordinate System

The accurate numerical representation of boundary conditions, be it the body surface or the infinity boundary, is best accomplished when the boundary is such that it is coincident with some coordinate line. Under such circumstances the boundary may be made to pass through the points of a finite difference grid constructed on the coordinate lines. This eliminates the need for any interpolation of the dependent variables between points of the grid. The avoiding of interpolation is particularly important for boundaries with strong curvature or slope discontinuities, and for differential systems that produce large gradients in the vicinity of the boundaries. Thus the generation of a curvilinear coordinate system with coordinate lines coincident with all boundaries is an essential part of a numerical solution. Extensive use of the method of numerical generation of a curvilinear coordinate system due to Thompson, Thames and Mastin [2], has been made in the present work. The main idea of this method is to fill the computational domain enclosed between the body and the external boundary with intersecting coordinate lines in the physical (x,y) space.

Let $\xi = \xi(x,y)$ and $\eta = \eta(x,y)$ be two continuously differentiable functions of the Cartesian coordinates (x,y). Further, let $\eta = \eta_o$ = constant be the body contour, while $\eta = \eta_\infty$ = constant be the external boundary contour. The region $\eta_o \leq \eta \leq \eta_\infty$ must now be filled by intersecting coordinate curves ξ = constant and η = constant. Because of

the closed region under consideration it is natural to specify the determining differential equations for ξ and η as elliptic equations to be solved under the proper boundary conditions for ξ and η at the body and at the external boundary. Since the simplest elliptic equation is the Laplace Equation, we then pose the problem of solving the Laplace Equations for ξ and η with x and y as independent variables under the Dirichlet boundary conditions. Let Γ_1 be the curve defining the body contour $\eta = \eta_o$ and Γ_2 be the curve defining the outer boundary $\eta = \eta_\infty$ in the xy-plane as shown in Fig.1. The elliptic boundary value problem is then

$$\nabla^2 \xi = 0 \tag{2.1}$$

$$\nabla^2 \eta = 0 \tag{2.2}$$

$$\text{on } \Gamma_1: \quad \xi = f_o(x,y), \ \eta = \eta_o \tag{2.3}$$

$$\text{on } \Gamma_2: \quad \xi = f_\infty(x,y), \ \eta = \eta_\infty \tag{2.4}$$

The solutions of Eqs. (2.1) and (2.2) under the boundary conditions (2.3) and (2.4) can conveniently be obtained in those cases when η_o and η_∞ can be specified by simple analytic methods (such as a circle, ellipse, etc.). To obtain coordinates for arbitrary shaped bodies, it is convenient to transform the Eqs. (2.1) and (2.2) such that x and y are the dependent while ξ and η are the independent variables. This transformation is more easily performed for either two or three-dimensional coordinates by the method of tensor analysis and is detailed in Appendix B. Referring to Eqs. (B-13) and (B-14), we find that Eqs. (2.1) and (2.2) are equivalent to

$$g_{22} x_{\xi\xi} - 2g_{12} x_{\xi\eta} + g_{11} x_{\eta\eta} = 0 \tag{2.5}$$

$$g_{22} y_{\xi\xi} - 2g_{12} y_{\xi\eta} + g_{11} y_{\eta\eta} = 0 \tag{2.6}$$

where the variable subscripts denote partial differentiations and the g_{ij} is the metric tensor defined in Appendices A and B. The boundary conditions are now

$$\text{On } \Gamma_1^*: \quad x = F_1(\xi,\eta_o),\ y = F_2(\xi,\eta_o) \tag{2.7}$$

$$\text{On } \Gamma_2^*: \quad x = G_1(\xi,\eta_\infty),\ y = G_2(\xi,\eta_\infty) \tag{2.8}$$

where as shown in Fig. 2, Γ_1^* and Γ_2^* are the images of the body and the external boundary contours in the $\xi\eta$-plane.

The geometrical meaning of the transformed equations (2.5) and (2.6) is that the body and the external boundary contours in the xy-plane have been mapped on to the $\xi\eta$-plane which is rectangular. In other words, we can say, that the contours in the xy-plane have been opened up to form the straight lines $\eta = \eta_o$ = constant, and $\eta = \eta_\infty$ = constant in the $\xi\eta$-plane. This can be achieved by imagining a cut connecting the body and the external boundary in the xy-plane as shown in Fig. 1., such that all functions and their derivatives are continuous in crossing the cut. Since a cut line is a part of the field, no boundary conditions can be imposed on Γ_3^* and Γ_4^* of Fig. 2.

The appearance of η_o and η_∞ in Eqs. (2.7) and (2.8) is now purely symbolic, denoting the names of the body and of the external boundary respectively. Given the body and the external boundary contours, we can always establish the values of x and y either graphically or analytically for any desired distribution of ξ-values. The η-values can be chosen arbitrarily to form rectangular meshes in the $\xi\eta$-plane.

Equations (2.5) and (2.6) are the basic equations for the generation of coordinates. To have a control over the spacing of the ξ and η lines, we envisage another general transformation, say from

ξ,η to ξ' and η'. Retaining the ξ,η notation, the equations take the form

$$g_{22}\, x_{\xi\xi} - 2g_{12}\, x_{\xi\eta} + g_{11}\, x_{\eta\eta} = \overline{P} x_{\xi} + \overline{Q} x_{\eta} \tag{2.9}$$

$$g_{22}\, y_{\xi\xi} - 2g_{12}\, y_{\xi\eta} + g_{11}\, y_{\eta\eta} = \overline{P} y_{\xi} + \overline{Q} y_{\eta} \tag{2.10}$$

For details on the above derivations refer to [8]. The same form of equations are obtained if one starts considering the Poisson Equations in place of Eqs. (2.1) and (2.2) and inverts the transformation from x,y to ξ,η as independent variables.

The function $\overline{P}$ and $\overline{Q}$ are to some extent arbitrary and can be chosen in various ways to have a desired distribution of coordinates in a given region. In the present research we have made $\overline{P}$ and $\overline{Q}$ to depend on the density gradients to contract the coordinates in the region of the shock. The chosen forms of $\overline{P},\overline{Q}$ are [9]

$$\overline{P} = g \sum_{k=1}^{n'} A_k' \operatorname{sgn}(\xi-\xi_k) \exp(-D_k'|\xi-\xi_k|) + g \sum_{\ell=1}^{m'} B_\ell' \operatorname{sgn}(\xi-\xi_\ell) \exp(-E_\ell' R_\ell) \tag{2.11}$$

$$\overline{Q} = g \sum_{k=1}^{n} A_k \operatorname{sgn}(\eta-\eta_k) \exp(-D_k|\eta-\eta_k|) + g \sum_{\ell=1}^{m} B_\ell \operatorname{sgn}(\eta-\eta_\ell) \exp(-E_\ell R_\ell) \tag{2.12}$$

where

$$g = g_{11}\, g_{22} - (g_{12})^2 = J^2 \tag{2.13}$$

$$R_\ell = [(\xi-\xi_\ell)^2 + (\eta-\eta_\ell)^2]^{1/2} \tag{2.14}$$

The first terms on the right hand sides of both (2.11) and 2.12) are used in the line attraction, while the second terms in both equations

are used for the point-attraction. Various terms which appear in these equations have been defined in the "List of Symbols".

In the present research, we have used only the point attraction term of Eq. (2.12) to concentrate the coordinate lines near the shock. The amplitude factor is a function of the maximum density difference along each ξ-line in the region of the shock. This amplitude factor B_ℓ thus changes according to the position (ξ,η) and is defined as

$$B_\ell = (\text{constant})\ (\rho_2-\rho_1)/\rho_1 \tag{2.15}$$

where the subscripts 1 and 2 denote the respective values in the front and behind of that shock which has been computed without coordinate contraction. The constant appearing in (2.15) is selected by trial and error and retains the same value for all ξ and η positions, that correspond to the shock location.

The method of numerical coordinate generation offers much freedom in the orientation of both the ξ and η coordinates in the physical xy-plane. For example, the η = const. lines can be chosen to go round the body as shown in Fig. 1, or they may not be chosen to form a complete circuit as shown in Fig. 5. However, a suitable choice has to be made in advance of computing the coordinates, because the resulting configuration of the body segment, the cut lines, or the re-entrant segments, and the outer boundary segments in the transformed $\xi\eta$-plane depend on this choice. In the present research we have chosen the coordinate configuration as shown in Fig. 3, in which the front outer boundary is a hyperbolic arc and the rear outer boundary is a circular arc. Figure 6 shows the corresponding segment orientation in the $\xi\eta$-plane. This type of segments orientation requires much care in

the computer programing for both the coordinate generation and for the numerical solution of the Navier-Stokes Equations. In Section 2.2 the finite-difference approximations of all the equations have been discussed.

2.2. Finite Difference Approximation

In this section the finite difference approximations and the numerical methods used for the solution of the elliptic systems, Eqs. (2.9) - (2.10) is discussed.

Before proceeding with the pertinent method of solution, it is important to mention that in the method of body-fitted coordinates it is superfluous to specify the step sizes $\Delta\xi$ and $\Delta\eta$, both of which are equal to 1. If IMAX and JMAX represent integers for the maximum numbers of ξ and η points respectively in a field, then this input and the desired contraction controlled by the amplitude and decay factors of Eqs. (2.11) - (2.12) decide the variable mesh sizes to be obtained by solving the generating system (2.9) - (2.10). This aspect has been thoroughly discussed in [8]. Thus the main utility of numerically generated body-fitted coordinates actually lies in the availability of meshes or nets in the $\xi\eta$-plane on which the Navier-Stokes Equations are to be solved without specifying the step sizes. Further, the variations both along the ξ-and η-coordinates, are labeled by the consecutive integers in the range $1 \leq I \leq IMAX$ and $1 \leq J \leq JMAX$.

The solutions of Eqs. (2.9) - (2.10) have been obtained by the Gauss-Siedel method with successive over relaxation (SOR) under the prescribed boundary values for x and y on the body and the external boundary contours, along with the prescribed values of IMAX and JMAX.

The spatial derivatives are approximated by the central differences

$$(\lambda_\xi)_{I,J} = (\lambda_{I+1,J} - \lambda_{I-1,J})/2 \tag{2.16}$$

$$(\lambda_{\xi\xi})_{I,J} = (\lambda_{I+1,J} - 2\lambda_{I,J} + \lambda_{I-1,J}) \tag{2.17}$$

where λ is a surrogate variable and I,J denote positions along ξ and η coordinates respectively. Similar expressions are obtained for λ_η, $\lambda_{\eta\eta}$ and $\lambda_{\xi\eta}$.

The solutions of Eqs. (2.9) - (2.10) yield x and y for the whole flow field as functions of ξ and η. This data is then used to generate the derivatives x_ξ, x_η, y_ξ, y_η, the metrical coefficients g_{ij}, the determinant g, and the Christoffel symbols Γ^i_{jk}.

It was mentioned in Section 2.1. that the orientation of the coordinates of the form shown in Fig. 5 requires due care in obtaining derivatives on the cut line. Referring to the schematic shown in Fig. 3 with the x-axis oriented along the cut line, let I_{UC} and I_{LC} denote the integral values of I on the upper and lower parts of the cut respectively. Thus

$$I_{LC} + I_{UC} = IMAX + 1 \ . \tag{2.18}$$

Equation (2.18) establishes the following correspondence between I_{LC} and I_{UC}:

I_{LC}		I_{UC}
1	Corresponds to	IMAX
2	" "	IMAX-1
:		
I	" "	IMAX-I+1
:		
I_{B1}	" "	I_{B2}

(2.19)

where I_{B1} and I_{B2} represent the same point of the body reached by the lower and upper parts of the cut respectively. Obviously

$$I_{B2} = (IMAX + 1) - I_{B1} .$$

From (2.19), we conclude that

$$x(I_{UC},J) = x(I_{LC},J) \tag{2.20}$$

and

$$x(I_{UC}+1,J) = x(I_{LC}-1,J) \tag{2.21}$$

The first derivatives on the lower and upper parts of the cut are

$$\begin{aligned}
(x_\xi)_{LC} &= \frac{1}{2}\,[x(I_{LC}+1,1) - x(I_{LC}-1,1)] \\
(x_\eta)_{LC} &= \frac{1}{2}\,[x(I_{LC},2) - x(I_{UC},2)] \\
(y_\xi)_{LC} &= \frac{1}{2}\,[y(I_{LC}+1,1) - y(I_{LC}-1,1)] \\
(y_\eta)_{LC} &= \frac{1}{2}\,[y(I_{LC},2) - y(I_{UC},2)]
\end{aligned} \tag{2.22}$$

where $2 \le I_{LC} \le I_{B1} - 1$.

$$\begin{aligned}
(x_\xi)_{UC} &= \frac{1}{2}\,[x(I_{UC}+1,1) - x(I_{UC}-1,1)] \\
(x_\eta)_{UC} &= \frac{1}{2}\,[x(I_{UC},2) - x(I_{LC},2)] \\
(y_\xi)_{UC} &= \frac{1}{2}\,[y(I_{UC}+1,1) - y(I_{UC}-1,1)] \\
(y_\eta)_{UC} &= \frac{1}{2}\,[y(I_{UC},2) - y(I_{LC},2)]
\end{aligned} \tag{2.23}$$

where

$$I_{B2} + 1 \le I_{UC} \le IMAX - 1 .$$

Using (2.21), in (2.23), we find that

$$(x_\xi)_{UC} = - (x_\xi)_{LC}$$

$$(y_\xi)_{UC} = - (y_\xi)_{LC} = 0$$

$$(x_\eta)_{UC} = - (x_\eta)_{LC} = 0$$

$$(y_\eta)_{UC} = - (y_\eta)_{LC} \qquad (2.24)$$

From the definition of Γ^i_{jk} given in Eq. (B-6) we find that on the cut line

$$\Gamma^1_{12} = \Gamma^2_{11} = \Gamma^2_{22} = 0 \qquad (2.25)$$

CHAPTER III

THE NAVIER-STOKES EQUATIONS

3.1. Formulation of the Problem

For solving the blunt body problem in general curvilinear coordinate system, we consider the nondimensionalized Navier-Stokes system of equations in the invariant tensor form. The conservation equations are

Mass Conservation:

$$\frac{\partial \rho}{\partial t} + \operatorname{div}(\rho \underset{\sim}{v}) = 0 \tag{3.1}$$

Momentum Conservation:

$$\frac{\partial}{\partial t}(\rho \underset{\sim}{v}) + \operatorname{div} \tilde{\tau} = 0 \tag{3.2}$$

Energy Conservation:

$$\frac{\partial \Psi}{\partial t} + \operatorname{div} \underset{\sim}{b} = 0 \tag{3.3}$$

where

$$\tilde{\tau} = \rho \underset{\sim}{v}\underset{\sim}{v} + p\tilde{I} - \varepsilon\tilde{\sigma}$$

$$\underset{\sim}{b} = (\Psi + p)\underset{\sim}{v} - \varepsilon\tilde{\sigma}\cdot\underset{\sim}{v} - \alpha_0 \mu \operatorname{grad} T$$

$$\Psi = \rho e + \frac{1}{2}\rho |\underset{\sim}{v}|^2$$

$$\tilde{\sigma} = K\tilde{I} + \tilde{d}$$

$$K = \lambda \operatorname{div} \underset{\sim}{v}$$

$$\tilde{d} = \mu \operatorname{def} \underline{v} = \mu[\operatorname{grad} \underline{v} + (\operatorname{grad} \underline{v})^T]$$

$$\varepsilon = 1/R_e$$

$$\alpha_0 = \varepsilon/P_r(\gamma-1)M_\infty^2 \tag{3.4}$$

The nondimensionalized equations (3.1) - (3.4) have been obtained by referring all lengths to the diameter $2R_n^*$; velocity vector, density, viscosity, temperature, enthalpy and pressure to the free stream values V_∞^*, ρ_∞^*, μ_∞^*, T_∞^*, h_∞^*, and $\rho_\infty^* V_\beta^{*2}$ respectively. The N-S Equations (3.1) - (3.4) by themselves do not give a complete description of the motion of a compressible fluid because changes in pressure and density cause temperature variations and thermodynamic principles must, therefore, enter into the considerations. Assuming the gas to be calorically and thermally perfect, the equation of state in the nondimensional variables is

$$p = \frac{\rho T}{\gamma M_\infty^2} \tag{3.5}$$

where γ is the adiabatic exponent. Similarly, the nondimensional temperature is given by

$$T = \gamma(\gamma-1)M_\infty^2 \left(\frac{\Psi}{\rho} - \frac{1}{2}|\underline{v}|^2\right) \tag{3.6}$$

The relation between temperature and viscosity is provided by the Sutherland formula, which in nondimensional form is

$$\mu = \frac{(1+S_1)T^{3/2}}{T + S_1} \tag{3.7}$$

where $S_1 = \dfrac{S_1^*}{T_\infty^*}$, $S_1^* = 110°K$.

Since Ψ is a function of T, hence the system of equations (3.1) - (3.7) form a closed system of equations provided $\lambda = \lambda(\mu)$ is also prescribed. In the present formulation we have used the Stokes' condition

$$3\lambda + 2\mu = 0 \tag{3.8}$$

as the required relation.

The boundary conditions for the system of equations (3.1) - (3.3) at the body surface are: $|\underset{\sim}{v}| = 0$, $T = T_w$, or $(\frac{\partial T}{\partial n})_w$ specified

$$\Psi_w = \frac{T_w \rho_w}{\gamma(\gamma-1)M_\infty^2}$$

$$p_w = \frac{\rho_w T_w}{\gamma M_\infty^2} \tag{3.9}$$

at free stream infinity: $|\underset{\sim}{v}| = 1$, $\rho = 1$, $T = 1$

$$p = \frac{1}{\gamma M_\infty^2}$$

$$\Psi = \frac{1}{2} + \frac{1}{\gamma(\gamma-1)M_\infty^2}$$

In (3.9) the subscript w denotes the wall condition. The density ρ_w is not known in advance but must be obtained by the equations themselves.

Since the governing equations are of parabolic-elliptic type, we therefore need to specify the outflow boundary conditions. In place of specifying the derivative conditions, we have used the complete solution of the Euler Equations to specify the downstream boundary condition with the stipulation that at the outer downstream boundary the effect of viscosity is negligible.

3.2. Transformation of the Equations

The governing equations (3.1) - (3.3) are now transformed to a general coordinate system $\xi^i (i = 1,2)$ by the method of tensor analysis (Appendix A). Using the summation convention on repeated indices, and introducing the new dependent variables

$$\sigma = \sqrt{g}\ \rho,\ P = \sqrt{g}\ p,\ D^{ij} = \sqrt{g}\ d^{ij},\ E = \sqrt{g}\ \psi \tag{3.10}$$

the equations are

$$\frac{\partial \sigma}{\partial t} + \frac{\partial}{\partial \xi^i}(\sigma v^i) = 0 \tag{3.11}$$

$$\frac{\partial}{\partial t}(\sigma v^i) + \frac{\partial}{\partial \xi^j}(\sigma v^i v^j) + \Gamma^i_{jk}\sigma v^j v^k = -\frac{\partial}{\partial \xi^j}(P g^{ij})$$

$$- P\,\Gamma^i_{jk} g^{jk} + \varepsilon\{\frac{\partial}{\partial \xi^j}(K\sqrt{g}\ g^{ij})$$

$$+ \frac{\partial D^{ij}}{\partial \xi^j} + \Gamma^i_{jk}(\sqrt{g}\ K g^{jk} + D^{jk})\} \tag{3.12}$$

$$\frac{\partial E}{\partial t} + \frac{\partial}{\partial \xi^i}\{(E + P)v^i\} = \varepsilon \frac{\partial}{\partial \xi^i}(\sqrt{g}\ \nu^i) + \alpha_0 \frac{\partial}{\partial \xi^i}(\mu\sqrt{g}\ g^{ij}\frac{\partial T}{\partial \xi^j}) \tag{3.13}$$

where g_{ij} is the transformation metric tensor, and

$$\nu^i = K v^i + \mu(g^{ik} g_{jm} v^j_{,k} + v^i_{,m})v^m \tag{3.14}$$

In Eqs. (3.10) - (3.14), the superscript indices denote the contravariant components, while a comma denotes the covariant differentiation, i.e.,

$$v^i_{,j} = \frac{\partial v^i}{\partial \xi^j} + \Gamma^i_{jk} v^k \tag{3.15}$$

where Γ^i_{jk} is the Christoffel symbol.

Equations (3.11) - (3.13) are applicable both to two and three space dimensions. In two dimensions, writing for brevity

$$\xi^1 = \xi,\ \xi^2 = \eta,\ v^1 = u,\ v^2 = v$$

$$A = \sigma u,\ B = \sigma v,\ H = \sigma(u)^2,\ M = \sigma(v)^2,\ N = \sigma uv, \tag{3.16}$$

$$Q = (E+P)u,\ R = (E+P)v$$

the equations become of the form

$$\frac{\partial \sigma}{\partial t} + \frac{\partial A}{\partial \xi} + \frac{\partial B}{\partial \eta} = 0 \tag{3.17}$$

$$\frac{\partial A}{\partial t} + \frac{\partial H}{\partial \xi} + \frac{\partial N}{\partial \eta} + \Gamma^1_{11}H + 2\Gamma^1_{12}N + \Gamma^1_{22}M = \theta \tag{3.18}$$

$$\frac{\partial B}{\partial t} + \frac{\partial N}{\partial \xi} + \frac{\partial M}{\partial \eta} + \Gamma^2_{11}H + 2\Gamma^2_{12}N + \Gamma^2_{22}M = \phi \tag{3.19}$$

$$\frac{\partial E}{\partial t} + \frac{\partial Q}{\partial \xi} + \frac{\partial R}{\partial \eta} = \psi \tag{3.20}$$

The expanded form of various terms appearing in Equations (3.17) - (3.20) are given in Appendix A.

The boundary conditions for Equations (3.17) - (3.20) are at the body surface: $u = v = 0$, $T = T_w$, or $(\frac{\partial T}{\partial n})_w$ specified

$$E_w = \frac{T_w \sigma_w}{\gamma(\gamma-1)M_\infty^2}$$

$$P_w = (\gamma-1)E_w ,$$

at free stream infinity: $u \to y_\eta/\sqrt{g}$, $v \to -y_\xi/\sqrt{g}$

$$\sigma \to \sqrt{g}$$

$$T \to 1$$

$$P \to \sqrt{g}/\gamma M_\infty^2$$

$$E \to \sqrt{g}\left(\frac{1}{2} + \frac{1}{\gamma(\gamma-1)M_\infty^2}\right) , \tag{3.22}$$

where a ξ or η subscript implies partial differentiation.

The local Mach Number M_ℓ is given by

$$M_\ell = M_\infty |\underset{\sim}{v}| / \sqrt{T} \tag{3.23}$$

where

$$|\underset{\sim}{v}|^2 = g_{11}(u)^2 + 2g_{12}uv + g_{22}(v)^2 \tag{3.24}$$

and

$$T = \gamma(\gamma-1)M_\infty^2 \left(\frac{E}{\sigma} - \frac{1}{2} |\underset{\sim}{v}|^2\right) \tag{3.25}$$

The relations between the local Cartesian and the local contravariant components of the velocity vector $\underset{\sim}{v}$ are

$$U = ux_\xi + vx_\eta$$
$$V = uy_\xi + vy_\eta \ . \tag{3.26}$$

The vorticity ω is given by the formula

$$\omega = \frac{1}{\sqrt{g}} \left(\frac{\partial v_2}{\partial \xi} - \frac{\partial v_1}{\partial \eta}\right) \tag{3.27}$$

where v_i are the covariant components of $\underset{\sim}{v}$, which are related with the contravariant components as

$$v_i = g_{ij} v^j = g_{i1} u + g_{i2} v \ . \tag{3.28}$$

The pressure coefficient is defined as

$$C_p = \frac{p^* - p_\infty^*}{\frac{1}{2} \rho_\infty^* V_\infty^{*2}} = 2\left(p - \frac{1}{\gamma M_\infty^2}\right) \tag{3.29}$$

CHAPTER IV

NUMERICAL SOLUTION OF THE N-S EQUATIONS

4.1. Navier-Stokes Algorithm

The Navier-Stokes Equations (3.17) - (3.20) can be put in the numerical vector form as

$$\frac{\partial \underline{w}}{\partial t} + \frac{\partial \underline{F}}{\partial \xi} + \frac{\partial \underline{G}}{\partial \eta} + \underline{H} = 0 \tag{4.1}$$

where

$$\underline{w} = \begin{Bmatrix} \sigma \\ A \\ B \\ E \end{Bmatrix} \tag{4.2}$$

$$\underline{F} = \begin{Bmatrix} A \\ H \\ N \\ Q \end{Bmatrix} \tag{4.3}$$

$$\underline{G} = \begin{Bmatrix} B \\ N \\ M \\ R \end{Bmatrix} \tag{4.4}$$

$$\underline{H} = \begin{Bmatrix} \Gamma^1_{11} H + 2\Gamma^1_{12} N + \Gamma^1_{22} M - \theta \\ \Gamma^2_{11} H + 2\Gamma^2_{12} N + \Gamma^2_{22} M - \phi \\ -\psi \end{Bmatrix} \tag{4.5}$$

We now discretize Eq. (4.1) by a fully implicit difference approximation. The time derivative is approximated by a first-order backward difference at n+1, where n is the time step of size Δt, while the spatial derivatives are approximated by central differences. The system of equations are solved by point-SOR, which are

$$\underset{\sim}{w}^{n+1}_{I,J} = \underset{\sim}{w}^{n+1(p)}_{I,J} + \omega \underset{\sim}{R}_{I,J} \tag{4.6}$$

where ω is the relaxation parameter and the superscript (p) denotes values at the previous iteration. The function $\underset{\sim}{R}$ is

$$\underset{\sim}{R}_{I,J} = \underset{\sim}{w}^{n}_{I,J} - \underset{\sim}{w}^{n+1(p)}_{I,J} - \frac{\Delta t}{2}\{\underset{\sim}{F}^{n+1}_{I+1,J} - \underset{\sim}{F}^{n+1}_{I-1,J}$$

$$+ \underset{\sim}{G}^{n+1}_{I,J+1} - \underset{\sim}{G}^{n+1}_{I,J-1}\} - (\Delta t)\, \underset{\sim}{H}^{n+1}_{I,J} \tag{4.7}$$

where the values of $\underset{\sim}{w}$ in $\underset{\sim}{F}$, $\underset{\sim}{G}$ and $\underset{\sim}{H}$ are those which are the most recent values available from the previous iteration. Fully expanded forms of (4.7) are given in Appendix D.

4.2. η-Derivatives on the Cut

To find the η-derivatives on the cut, we refer to Figure 4. The point 1 of the physical plane (Figure 3) transforms to the location marked x on the transformed plane, while point 2 remains at its original position relative to the cut. Thus in principle, the function value at the fictitious point shown under the lower cut must be replaced by the function value at the point 2 on the upper cut. Now two cases arise depending on whether the function is a scalar or a vector.

For a scalar f, the first η-derivatives are

$$\left(\frac{\partial f}{\partial \eta}\right)_{I_{LC},1} = \frac{1}{2}\left[f(I_{LC},2) - f(I_{UC},2)\right]$$

$$\left(\frac{\partial f}{\partial \eta}\right)_{I_{UC},1} = \frac{1}{2}\left[f(I_{UC},2) - f(I_{LC},2)\right]$$

Thus

$$\left(\frac{\partial f}{\partial \eta}\right)_{I_{LC},1} = -\left(\frac{\partial f}{\partial \eta}\right)_{I_{UC},1} \tag{4.8}$$

Similarly, the second η-derivatives are

$$\left(\frac{\partial^2 f}{\partial \eta^2}\right)_{I_{LC},1} = f(I_{LC},2) - 2f(I_{LC},1) + f(I_{UC},2) \tag{4.9}$$

$$\left(\frac{\partial^2 f}{\partial \eta^2}\right)_{I_{UC},1} = f(I_{UC},2) - 2f(I_{UC},1) + f(I_{LC},2) \tag{4.10}$$

But f is a scalar, so that

$$f(I_{LC},1) = f(I_{UC},1)$$

hence both (4.9) and (4.10) represent the same value.

To find the η-derivatives of a directional quantity u on the cut, we need the value of u at the fictitious point. Since in the physical plane u in the lower part of the cut is directed opposite to that on the upper part of the cut, hence

$$\left(\frac{\partial u}{\partial \eta}\right)_{I_{LC},1} = \frac{1}{2}\left[u(I_{LC},2) - (-u(I_{UC},2))\right]$$

$$= \left(\frac{\partial u}{\partial \eta}\right)_{I_{UC},1} \tag{4.11}$$

The same holds for v, x_ξ, x_η, y_ξ and y_η.

Based on the preceding analysis it is easy to show that either for a scalar function f or a vector function y the derivatives across the cut are continuous.

4.3. Calculation of Wall Density

The wall density is calculated by evaluating each term of the continuity equation (3.17) at the body surface. Denoting by J=1 the body surface, we have

$$\left(\frac{\partial \sigma}{\partial t}\right)^{n+1}_{I,1} = - \left(\frac{\partial B}{\partial \eta}\right)^{n+1}_{I,1}$$

Using a three-point forward difference approximation for the right hand side, we obtain

$$\sigma^{n+1}_{I,1} = \sigma^{n}_{I,1} - \frac{\Delta t}{2} \left(4B^{n+1}_{I,2} - B^{n+1}_{I,3}\right) \tag{4.12}$$

where $B^{n+1}_{I,1} = 0$.

Though Eq. (4.12) is fully implicit, nevertheless its use at the trailing edge point always produces unrealistic density values. To circumvent this difficulty, Eq. (4.12) was used at all points of the body except at the trailing edge point where an explicit scheme based on the leap-frog method was used:

$$\left(\frac{\partial \sigma}{\partial t}\right)^{n}_{I,1} = - \left(\frac{\partial B}{\partial \eta}\right)^{n}_{I,1}$$

$$\frac{\sigma^{n+1}_{I,1} - \sigma^{n-1}_{I,1}}{2\Delta t} = - \frac{1}{2} \left(B^{n}_{I,2} - B^{n}_{I,0}\right)$$

where "0" is a fictitious point. Using a second order extrapolation in space and time, we get

$$B^{n}_{I,0} = 2B^{n-1}_{I,1} - B^{n-2}_{I,2}$$

Thus the wall density is obtained by the expression

$$\sigma^{n+1}_{I,1} = \sigma^{n}_{I,1} - \Delta t \left(B^{n}_{I,2} + B^{n-2}_{I,2}\right) \tag{4.13}$$

4.4. Nonlinear Instability

In the solution of compressible flow equations, several types of nonlinear instabilities are encountered. Among these, the most dominant is due to the difference approximation of the convective derivative. These instabilities can be avoided by introducing some dissipation in the difference approximation of the differential equation being solved. In this context, McCormack [10] has used a fourth-order damping term for his explicit schemes. Boris and Brook [11] have developed a flux-corrected transport (FCT) technique which is quite efficient for use in the continuity equation. Vliegenthart [7] and Harten and Zwas [12] have used "Shuman Filtering" to supress the convective instabilities.

In the present research both the FCT of Ref. [11] and the Shuman Filtering of Ref. [7] have been tried. Though the Shuman Filter adds more dissipation than desired, particularly near the shock, it always produced wiggle-free solutions for all regions of the flow field. The application of Shuman Filter amounts to replacing the flow variable $\bar{w}^n_{i,j}$, by $w^n_{i,j} = \sqrt{g}\,\bar{w}^n_{i,j}$, in 4.7, where

$$\bar{w}^n_{i,j} = (1/8)[\bar{w}^n_{i+1,j} + \bar{w}^n_{i-1,j} + \bar{w}^n_{i,j+1} + \bar{w}^n_{i,j-1} + 4\,\bar{w}^n_{i,j}] \qquad (4.14)$$

This scheme was used on all the four primary flow variables in the form of $\sigma/\sqrt{g}$, $A/\sqrt{g}$, $B/\sqrt{g}$ and $E/\sqrt{g}$. After Equation (4.14) was applied to these quantities the original dependent variables of the N-S Equations were recovered by multiplying each of the filtered variables by the Jacobian, $\sqrt{g}$. This filtering technique was carried out on the converged solution that was obtained at the end of 5 time steps, each time step (Δt) being 0.01. The frequency of application of the Shuman Filter had to be determined by trial and error.

4.5. Downstream Boundary Conditions

For the solution of the parabolic-elliptic system of Equations (3.17) - (3.20), beside the boundary conditions at the body surface and at the upstream free boundary (Eqs. 3.22)), it is also necessary to specify a proper set of conditions at the downstream boundary. To obtain these conditions, the downstream boundary was placed at a sufficient distance where the viscous dissipation is negligibly small and the complete Euler's Equations were solved on the entire downstream boundary. The computer program has been structured in such a way that it solves both the Navier-Stokes and Euler's Equations with each iteration.

The Euler Equations that were solved on the downstream boundary, at each iteration, are:

$$\frac{\partial \sigma}{\partial t} + \frac{\partial A}{\partial \xi} + \frac{\partial B}{\partial \eta} = 0 \tag{4.15}$$

$$\frac{\partial A}{\partial t} + \frac{\partial H}{\partial \xi} + \frac{\partial N}{\partial \eta} + [\Gamma^1_{11} H + 2\Gamma^1_{12} N + \Gamma^1_{22} M]$$

$$= (1/g)[g_{12} \frac{\partial P}{\partial \eta} - g_{22} \frac{\partial P}{\partial \xi}] + (P/g)[g_{22}(\Gamma^1_{11} + \Gamma^2_{12})$$

$$- g_{12} (\Gamma^1_{12} + \Gamma^2_{22})] \tag{4.16}$$

$$\frac{\partial B}{\partial t} + \frac{\partial N}{\partial \xi} + \frac{\partial M}{\partial \eta} + [\Gamma^2_{11} H + 2\Gamma^2_{12} N + \Gamma^2_{22} M]$$

$$= (1/g)[g_{12} \frac{\partial P}{\partial \xi} - g_{11} \frac{\partial P}{\partial \eta}] + (P/g)[g_{11}(\Gamma^1_{12} + \Gamma^2_{22})$$

$$- g_{12} (\Gamma^1_{11} + \Gamma^2_{12})] \tag{4.17}$$

$$\frac{\partial E}{\partial t} + \frac{\partial Q}{\partial \xi} + \frac{\partial R}{\partial \eta} = 0 \tag{4.18}$$

The finite-differencing of these equations was carried out by three-point forward-differencing in the ξ direction on the $\xi = 1$ coordinate and by three-point backward-differencing in the ξ direction on the $\xi = \xi_{max}$ coordinate. Central differences were used for the η derivatives.

4.6. Coordinate Contraction Near a Shock

The capability of attracting the coordinate lines to other pre-designated coordinate lines or grid points exists at present and through the application of this technique to blunt body flows with strong shocks an effort was made to concentrate in, and define, the region of the shock. The magnitude of concentration is controlled by the factors B_ℓ and E_ℓ defined in Eq. (2.12). These coordinate control factors were expressed as functions of the local density gradients across the shock as shown in Eq. (2.15). The equations for the generation of the coordinate system (Eqs. (2.9), (2.10), using coordinate control, were solved, as well as the Navier-Stokes Equations, when a quasi steady-state has been reached. This process was repeated after a pre-assigned number of time steps. Thus the coordinate system was refined in the region of the shock and moved with it. This measure reduced the need of having a very refined mesh in the entire computational domain by providing refinement only in the region through which the shock happened to be passing at any given time. However, it must be noted that this refinement near the shock was achieved at the expense of the accuracy near the wall where a finer mesh is always needed to resolve the boundary layer.

CHAPTER V

COMPUTATIONAL PROCEDURE AND RESULTS

5.1. Computational Procedure

The first step in the numerical solution of the transformed N-S Equations is the determination of the computational domain so that the appropriate boundary conditions may be prescribed around it. In the present case of super-sonic flow, the flow field remains unperturbed upstream of the bow shock wave, and the computational domain is limited upstream by a boundary located at a short distance ahead of the bow shock. The "stand-off" distance of this detached shock, for a given free stream Mach Number, is estimated using empirical equations [13]. On the upstream boundary the uniform flow conditions are used as boundary conditions. Particular care had to be taken to ensure that the bow shock did not cut across any segment of this upstream boundary. On the downstream boundary the boundary conditions varied with time and were determined by solving the Euler's Equations (cf. Chapter IV).

The computational domain and the profile of the body in it having been determined, the next step was the numerical generation of the coordinate system which has already been described. The cartesian coordinates of each of the mesh points in the entire computational domain having been determined and stored, the coefficients that occur in the Navier-Stokes Equaitons due to transforming them into general curvilinear coordinates could now be calculated and stored in a file.

The actual solution of the N-S Equations now starts with an assumed initial guess of the solution for the entire computational domain. These initial conditions need not necessarily be physically

realistic and when they are not, the transient solution has no physical meaning. In the present case the initial conditions chosen for the whole flow field were the uniform flow conditions that were prescribed on the upstream boundary. It was however found that this could not be done if the free stream Mach Number was very high, or if the isothermal temperature condition prescribed on the body was far different from the free stream value. The finite-difference scheme chosen was the S.O.R. which is an implicit scheme. The value of the optimum acceleration parameter for all the equations, i.e., continuity, momentum and energy, was determined, by trial, to be 0.9. In approximating the convective derivatives of these equations, the average of the product (A.O.P.) finite-difference scheme rather than the product of the average (P.O.A.) proved fruitful, even though it is generally considered that a non-linear instability can result in regions of flow reversal when the average of the product scheme is used.

The problem of the treatment of boundary conditions at an impermeable wall in viscous compressible flows reduces to that of the calculation of the pressure or of the density. In this research the wall density was calculated from the continuity equation written at the wall. Peyret and Viviand [4] report that such a technique is of delicate use and may lead to strong oscillations or even to divergence if no artificial viscosity term is added to the continuity equation; and that, in particular, in the case of separated flows negative values of the density may be obtained. This, in fact, was what happened at the trailing-edge point using the continuity equation. This problem was overcome by using an explicit discretization based on the leap-frog scheme, only at the trailing edge (cf. Eq. 4.13).

In general it was found that at a given time-step iterative convergence to the tolerance of 10^{-6} occurred in about 6 iterations. While carrying out these iterations the downstream boundary conditions varied with every iteration. Progress in time was made by increasing the time by a Δt of .01 at the end of each time step. The problem of wiggles was overcome by applying the Shumann filter at the end of every 5 time steps. Provision was made in the computer program to store the solution obtained at the end of any desired time step in a file; and the ability to read back from this storage file and to restart the program where it last left off was also incorporated. The computer program also locates and calculates the maximum change that occurs in a typical flow variable, such as density, along every ξ = constant line that passes through the region of the shock. Thus at the end of any pre-designated time step the location of the shock and the change in the density across it is automatically recorded. This information is used again if necessary in the generation of a new coordinate system wherein the coordinate attraction technique is used to refine the mesh in the immediate vicinity of the shock.

On an average it took 0.525 minutes of computer time (on a UNIVAC 1108) to achieve iterative convergence at each time step. The stand-off distance of the bow shock became quite constant after about 320 time steps, each increment in the characteristic time-step being equal to .01. All the cases were, however, run up to 400 time steps and the total computer time requirement to achieve this "steady-state" solution was about 2 hours and 30 minutes.

A reduction in the time-interval Δt should normally lead to more accurate results. The use of a filter, such as the Shuman filter, however, increases the dissipation with decreasing time-interval Δt. For the case of the clyinder, with a time-step of 0.005 the pressure distribution was generally found to be higher, particularly in the vicinity of the 90° point, i.e., the top of the cylinder. The use of the Flux Corrected Transport Filter was not quite satisfactory as it introduced too little dissipation, as opposed to the Shuman Filter which introduced too much. In fact, the Shuman Filter introduced so much artificial viscosity that it overshadowed the effect of a reduction in the free stream Reynolds Number. For the same Δt of 0.005 a reduction of Re from 100,000 to 10,000 made no difference to the solution. In general it was found that an increase in Reynolds Number required a smaller time-increment Δt.

5.2. Discussion of Results

The numerical solution of the complete Navier-Stokes Equations for a super-sonic flow was obtained for the flow about a two-dimensional circular cylinder. The uniform flow conditions used in the computations were $M_\infty = 4.6$, $Re_\infty = 10{,}000$, $T^*_\infty = 167°K$, $p^*_\infty = 14.93\ N/M^2$ and $P_r = 0.72$. For these free stream conditions the coefficient of viscosity works out to be $\mu^*_\infty = 1.13154 \times 10^{-5}$ kg/m-sec and the density $\rho^*_\infty = 3.11593 \times 10^{-4}$ kg/m^3. The ratio of the specific heats was assumed to be $\gamma = 1.40$. All calculations presented in this report have been performed for the isothermal wall temperature T^*_w of 556°K. The diameter of the circular cylinder was $2R^*_n = 0.3048m$. The Knudsen Number for a perfect gas is defined by the expression $\sqrt{\gamma\pi/2}\ (M_\infty/Re_\infty)$, which for the above free stream conditions is 6.821529×10^{-4}.

The graphical results presented correspond to the steady state solutions at a characteristic time of 3.20, with the exception of the Mach contour plots which are presented at two different periods of time so as to give an insight into the formation and progress of the bow shock wave as the solution of the N-S Equations advances in time towards a steady state.

Figure 5 shows the physical field, which constituted the computational domain and Figure 6 represents the transformed ξ-η field used in the numerical computations. In this transformed field the body extends from $\xi = 9$ to $\xi = 31$ on the lower side. The upstream boundary transforms to the line on the top while the two vertical sides represent the downstream boundary. A fairly compact field with 39 lines in the ξ-direction and 35 lines in the η-direction was used.

Even so the computer program required 62K of core capacity on a UNIVAC 1100 series computer. As the η-line spacing was already sparse to begin with, the scope for mesh refinement in the region of the shock was very much restricted. In Figure 7 the concentration of the η-lines in the region of the shock is exhibited.

Figures 8 and 9 are the Mach contour plots at the characteristic times of 0.8 and 3.2 and depict the progression of the bow shock wave from the body to its steady state stand-off distance. The Mach contour interval is 0.1. The sonic lines between the bow shock and the body, in which region the flow is wholly sub-sonic, are indicated in Figure 9. It can be seen from this figure that aft of the body too, a sub-sonic region exists which extends up to a distance of about 2 times the diameter of the cylinder from its center. Behind this sub-sonic region, the flow again is super-sonic. In the field shown in Figure 5, the computational domain downstream of the body was limited by a semi-circle of radius 2.5 and the boundary conditions on this exit plane, as mentioned in Sect. 4.5, were established by solving the Euler's Equations on it. Since the downstream boundary is located beyond the sub-sonic region and wholly in a super-sonic field of flow the use of the Euler's Equations is thus seen to be perfectly valid and accurate. In Figure 5 it can be noticed that the upstream boundary of the field starts and ends vertically above and below the clyinder respectively. This was dictated by the need of having to prescribe the free stream conditions at least up to those points. Figure 10 shows the Mach contours at time 3.2 for the field with mesh refinement.

Figures 11 through 18 depict the variation of density, pressure, temperature and velocity from the front stagnation point of the cylinder

to the upstream boundary along the symmetry line ($\xi = 20$) in the steady state. In the physical field the front stagnation point is located at $x = -0.5$ and the upstream boundary, on the line of symmetry, at $x = -1.25$. The absolute values of x are indicated in the plots. Figure 11 is the density distribution without mesh refinement, while 12 is the density variation with mesh refinement in the shock region. While the trend of density, pressure, temperature and velocity distributions seems satisfactory, the shock stand-off distance is more than what the ideal theories of Refs. [13] and [15] predict. This effect is due to the introduction of numerical dissipative terms, necessitated by the need to damp out wiggles. The disturbance of the smooth variation of the η-lines brought about by the mesh refinement seems to have given rise to the oscillations in the density, pressure, temperature and velocity profiles depicted in Figures 12, 14, 16, and 18 respectively. Considering the coordinate system to be independent of time could also have contributed to these oscillations.

Figure 19 shows the variation of the coefficient of pressure (C_p) along the upper half of the cylinder from the front stagnation point to the trailing edge, while in Figure 20, C_p is plotted for the field with mesh refinement.

Figures 21 and 22 show the distribution of wall pressures from 0° to 180° normalized with the stagnation value without and with mesh refinement respectively. The mesh refinement, mild as it is, has not made any appreciable change in the pressure distribution on top of the cylinder as seen from Figures 20 and 22. In Figure 23 the results plotted in Figure 21 are compared with the experimental results quoted in Ref. [5] up to the 90° point. It is seen that the numerical

solution of the compressible N-S Equations, for the free stream conditions considered, yields results which are quite in agreement with those obtained by experiments.

Figures 24 and 25 show the computational domain and the pressure distribution on a cylinder with a fairing for $M_\infty = 4.6$ and $Re = 10$. It is noticed that the pressure increases as we move closer to the 90° point, when compared with the results for the cylinder without a fairing.

CHAPTER VI

CONCLUSIONS

6.1. In general, in any numerical computational work, the finer the mesh system the more realistic the solution is expected to be, particularly in regions where large gradients are encountered. This fact was amply made clear in the present research where it was found that as the intensity of the η-line spacing around the cylinder was increased the pressure distribution on it progressively approached the experimental results.

6.2. It is also generally agreed upon that for any given intensity of the coordinate line spacing the farther the free stream boundary can be located from the body, the better the solution would be - subject to the limitations of computer time and storage. In the present investigation this factor was even more crucial as the bow shock tended to cut across the upstream boundary on which the free stream conditions were prescribed. Hence the upstream boundary was located as far upstream as we could and as parallel to the bow shock as possible, without compromising too much on the η-line spacing around the body.

6.3. The influence of the downstream flow conditions on the resultant flow field about a body in super-sonic flow seems to be a controversial topic. In this research for the same number of mesh points (39 x 35) various fields were considered in which the distance of the downstream boundary from the body varied, which in effect, varied the ξ-line spacing aft of the body. The best results were obtained for the boundary location that resulted in a finer ξ-line spacing, thus conclusively proving that downstream flow conditions do affect the

numerical solution even in high Mach Number flows. This point is discussed in detail by Roache [6].

6.4. The nearness of the downstream boundary to the body is not too detrimental so long as it is placed beyond the wake region aft of the body in which viscous effects do predominate and in which the flow is sub-sonic. The downstream boundary being located entirely in a super-sonic flow field, the Euler Equations may be used to establish accurately the downstream conditions.

6.5. The wall density, except at the trailing edge, was calculated from the continuity equation written at the wall, using three-point forward difference approximations. However at the trailing edge, or the rear stagnation point, an explicit discretization of the continuity equation based on the leap-frog scheme proved beneficial in overcoming the negative densities that were otherwise occurring there. The same scheme when applied to the rest of the body, however, drove the wall densities down progressively, until negative values appeared in the neighborhood of the leading edge.

6.6. Generally it is considered that a non-linear instability can result by using the average of the product (A.O.P.) scheme in approximating the convective derivatives, particularly in regions of flow reversal. In this research however, the A.O.P. scheme seemed to result in oscillations that were detrimental to the solution and thus the product of the average scheme was used.

6.7. Normally we would expect a better solution by refining the mesh in the region of the shock where very high gradients of the flow variables exist. In the present work mesh refinement in the shock region

caused oscillations to build up quite rapidly there, while the pressure distribution on the body itself remained unaffected. While no definite conclusions can be made at this stage, it is probable that the following factors caused the wiggles to appear in spite of the Shumann Filter.

(a) The η-line spacing in the computational domain was barely sufficient to start with; and the subsequent attraction of the η-lines into the region of the shock only caused a coarser mesh on either side of the shock.

(b) Abrupt variations in the coordinate line spacing are not conductive to good results. It is possible that the mesh refinement that was attempted could have caused such uneven η-line spacing.

(c) The solution could also be extremely sensitive to perturbations caused by the propagation of the shock by however small a distance, even though the mesh refinement was attempted at an almost steady-state stage of the solution.

To sum up the work done, the numerical solution of the full N-S Equations for viscous compressible flows with a detached bow shock ahead of a two-dimensional circular cylinder has been obtained. The results agree quite well with experiment. Besides quite a steady state solution was obtained in a very short characteristic time. Before a comparison of the efficiency of the method can be made in relation to any other, the following points should be kept in mind. The computational domain was small, 39 x 35 mesh points in all. Iterative convergence was obtained to a tolerance of 10^{-6} for all variables at each time step ($\Delta t = .01$), in 6 iterations on an average. The total computer time required to achieve a steady state solution on an UNIVAC

1100 series computer, inclusive of the time required to generate the numerical curvilinear coordinate system, the coefficients of the N-S Equations, etc., is about 3 hours. A larger computational domain and a finer mesh will no doubt yield a better solution. The range of Mach Numbers and Reynolds Numbers for which this scheme is valid is yet to be tested. Nevertheless, judging from the results obtained, it is believed that we are one more step ahead in using Computational Fluid Dynamics as a standard aerodynamic technique.

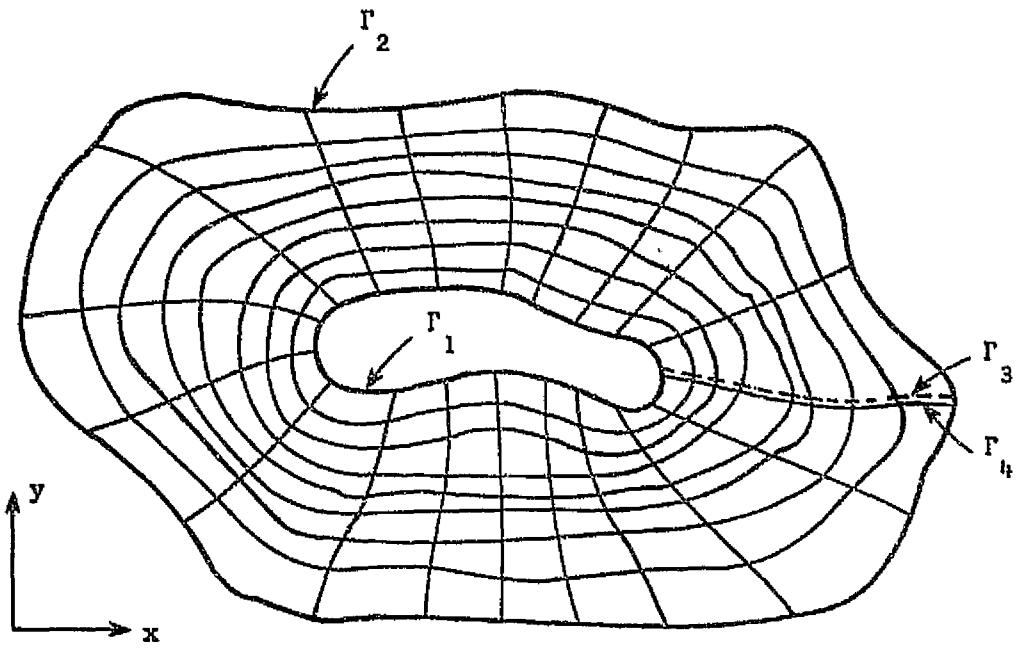

Figure 1. Physical Plane.

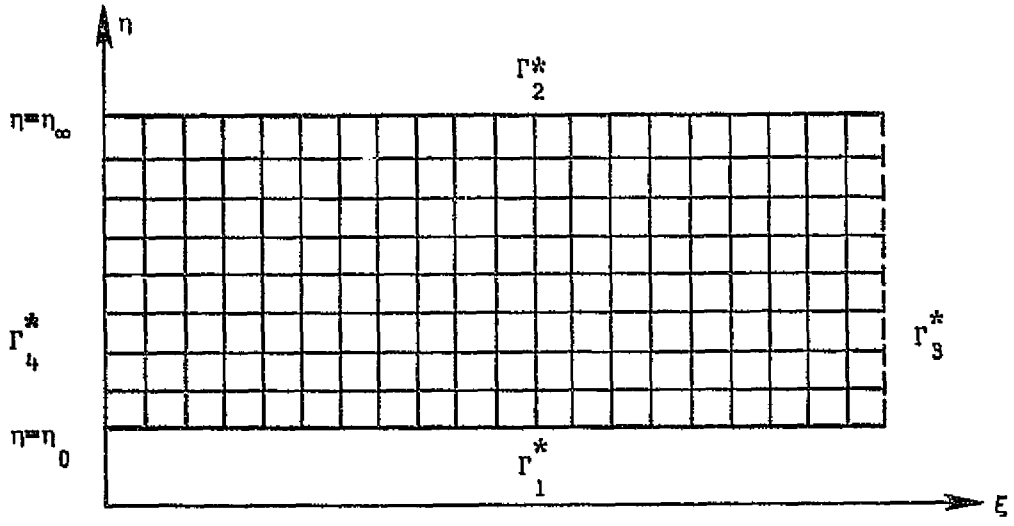

Transformed Plane
(Natural Coordinates)

Figure 2. Field Transformation.

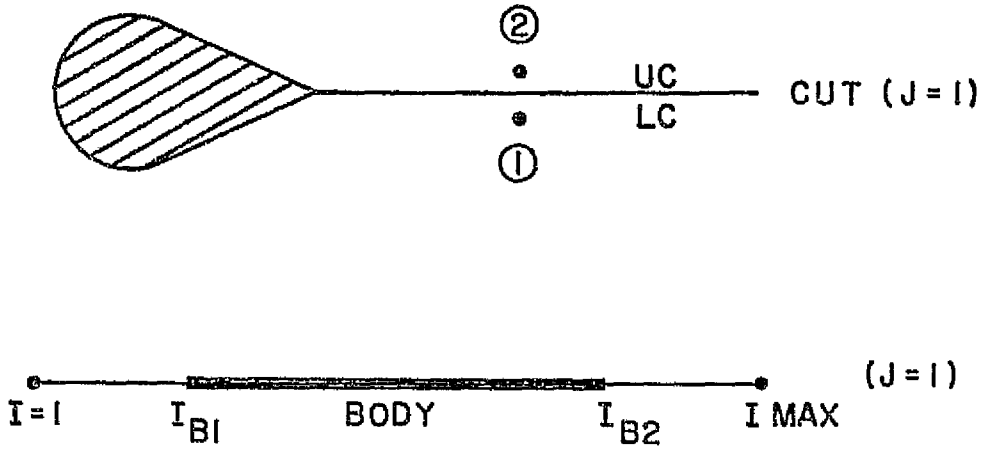

Figure 3. Grid Points Across a Cut in the Physical Plane

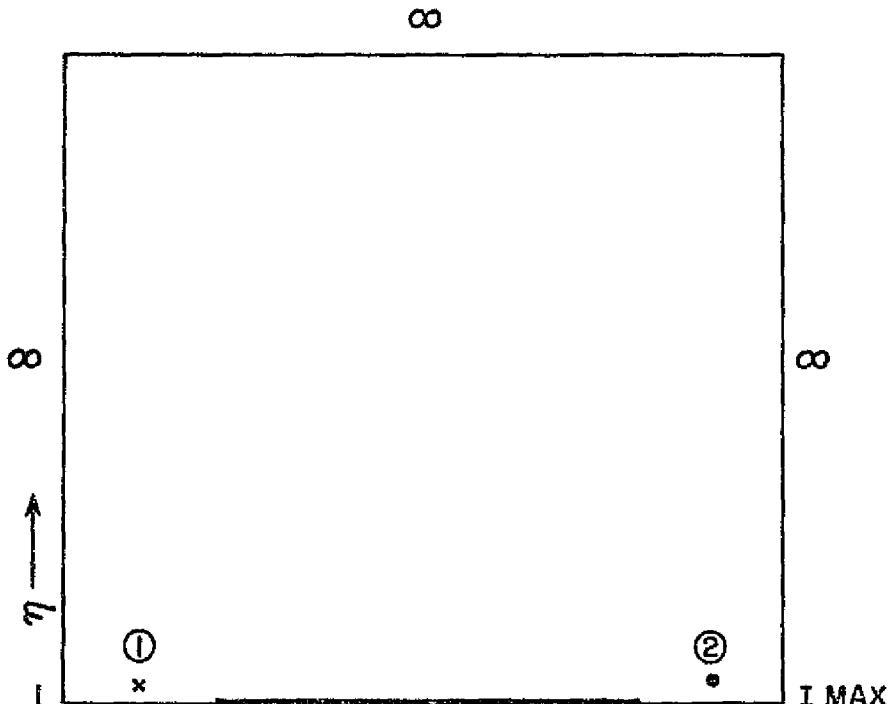

Figure 4. Grid Points Across a Cut in the Transformed Plane

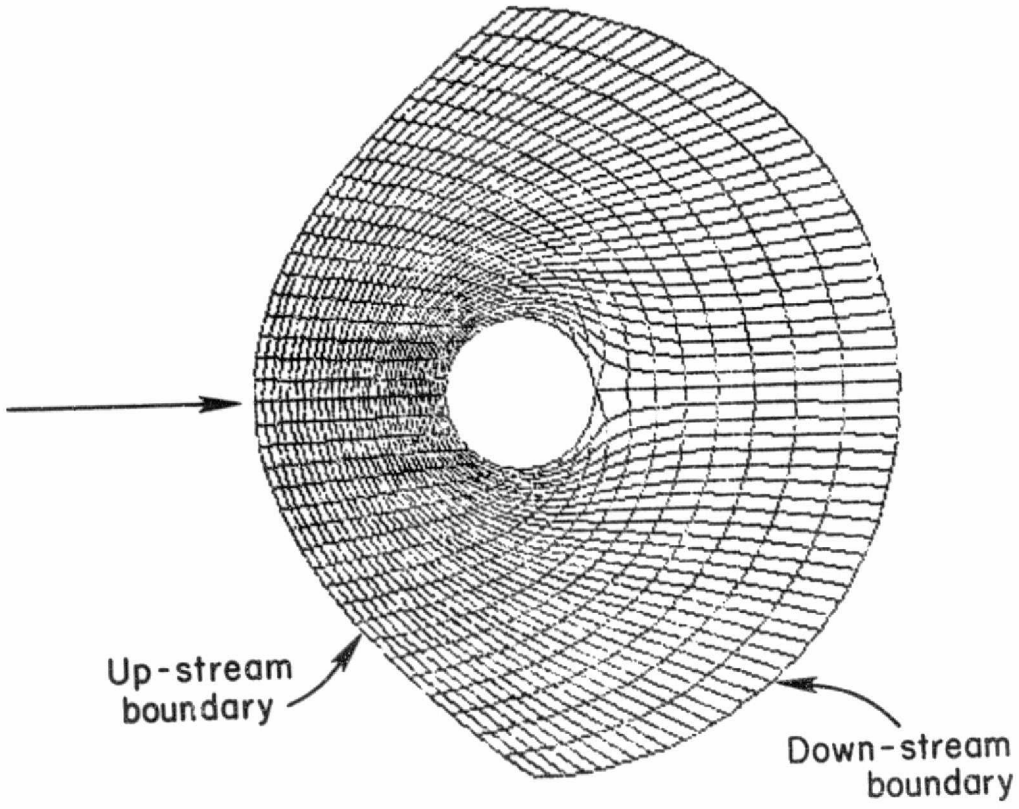

Figure 5. The Computational Domain

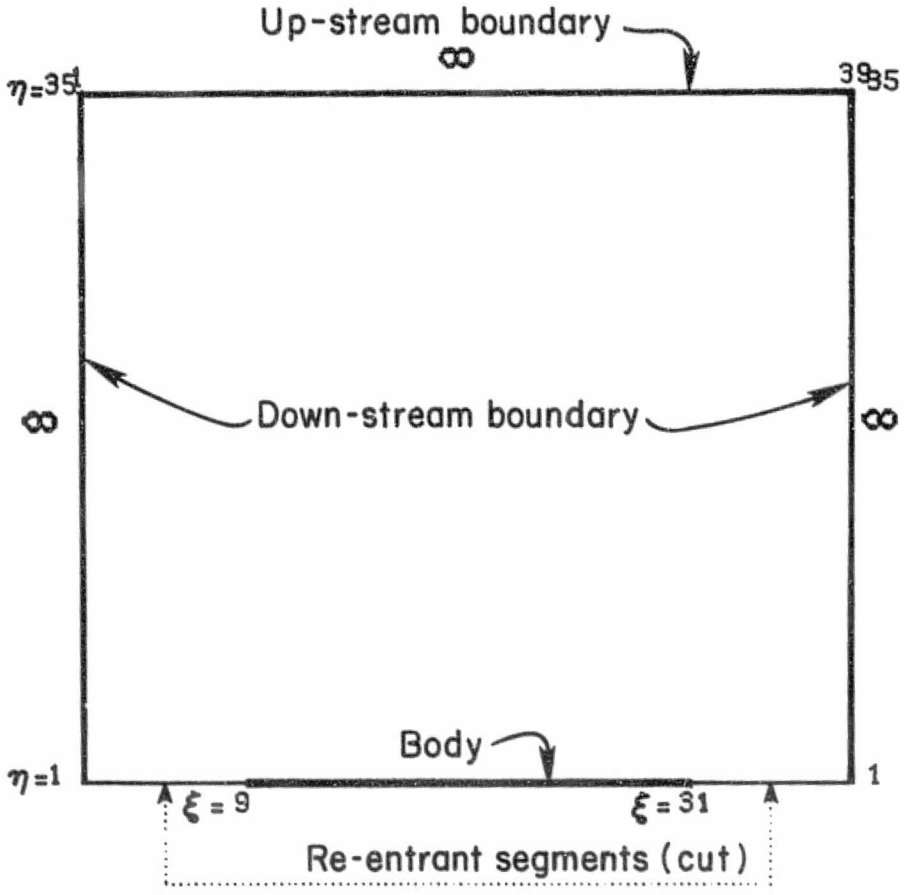

Figure 6. The Transformed Computational Domain.

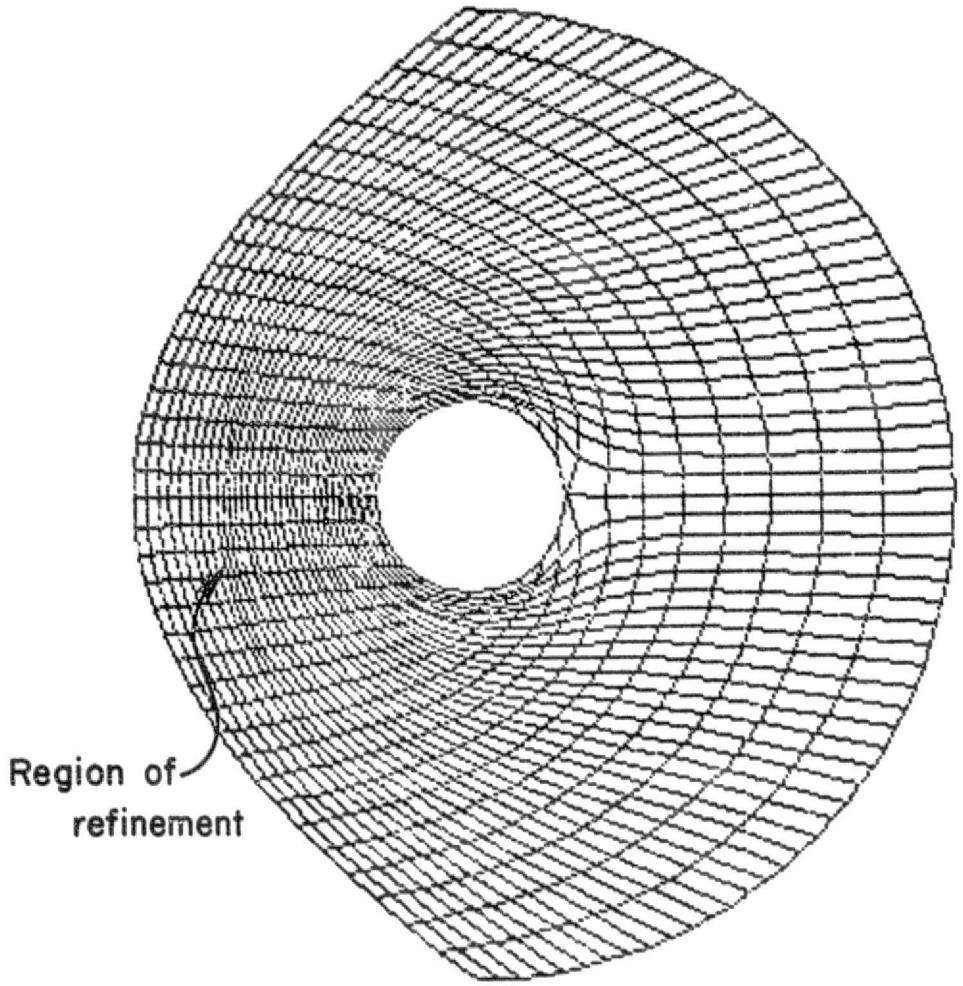

Figure 7. The Computational Domain with Mesh Refinement.

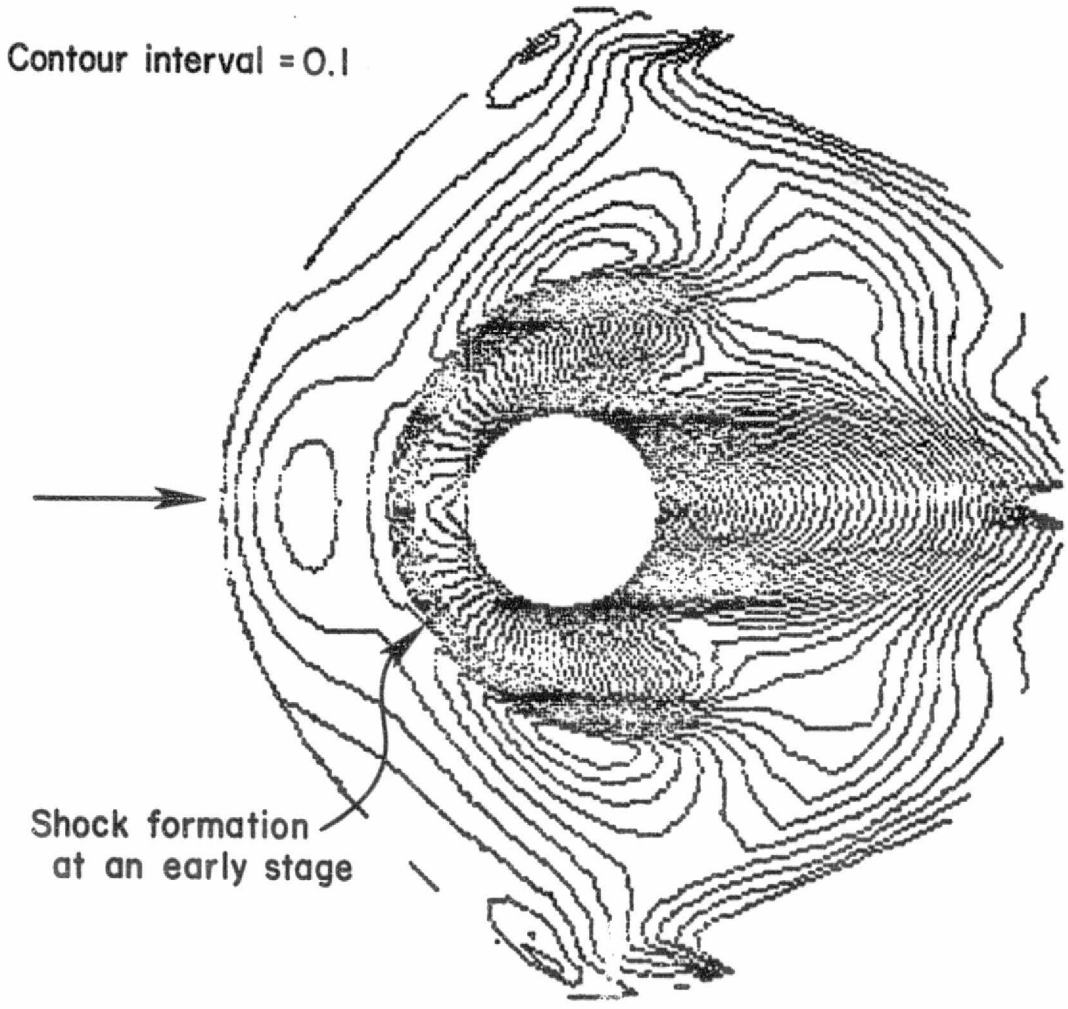

Figure 8. Mach Contours at Time 0.8.

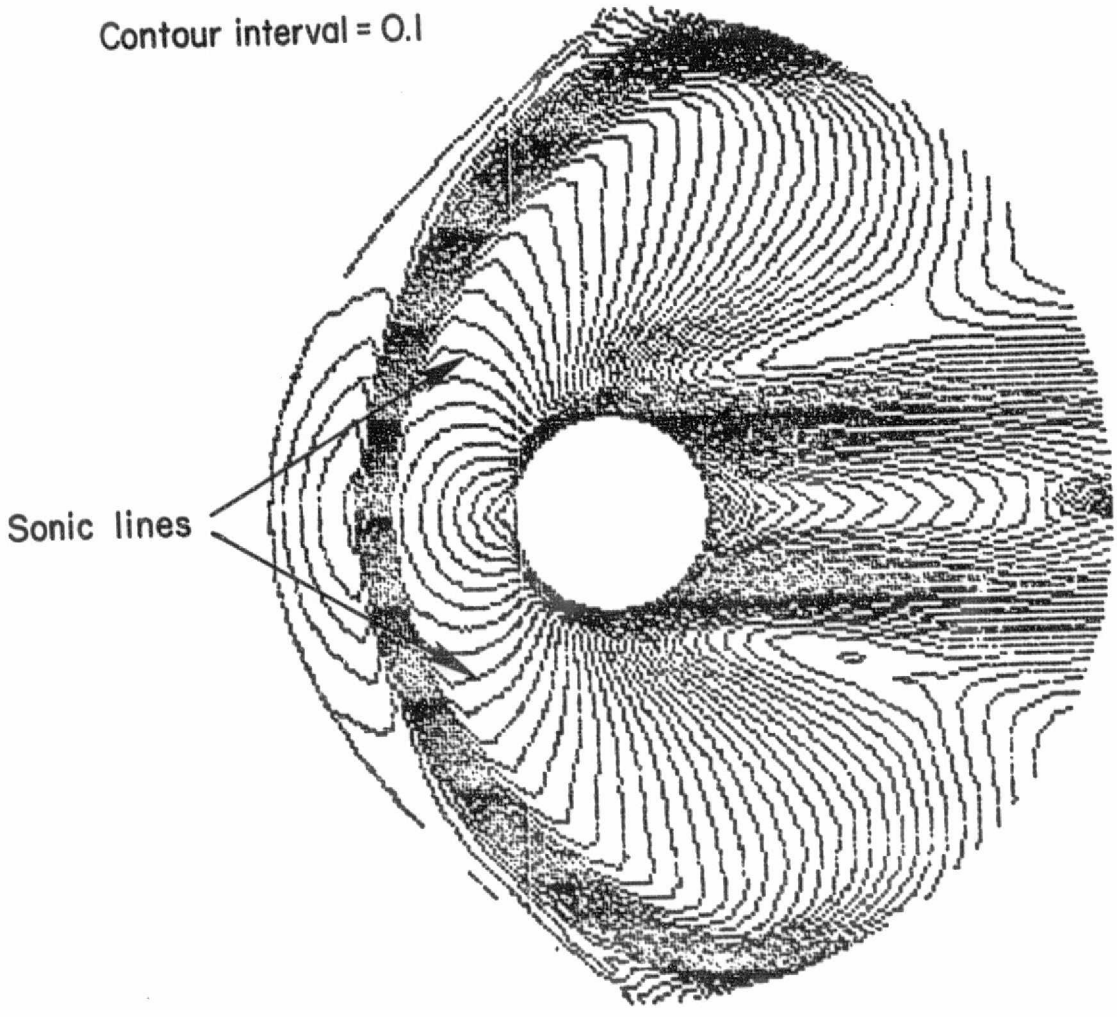

Figure 9. Mach Contours at Time 3.2.

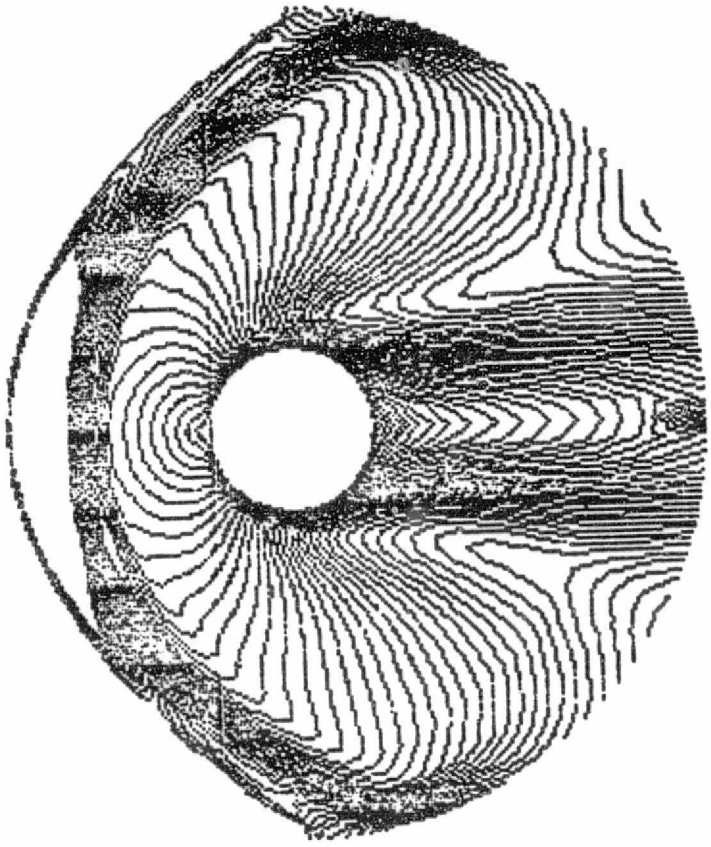

Figure 10. Mach Contours at Time 3.2 for Field with Mesh Refinement.

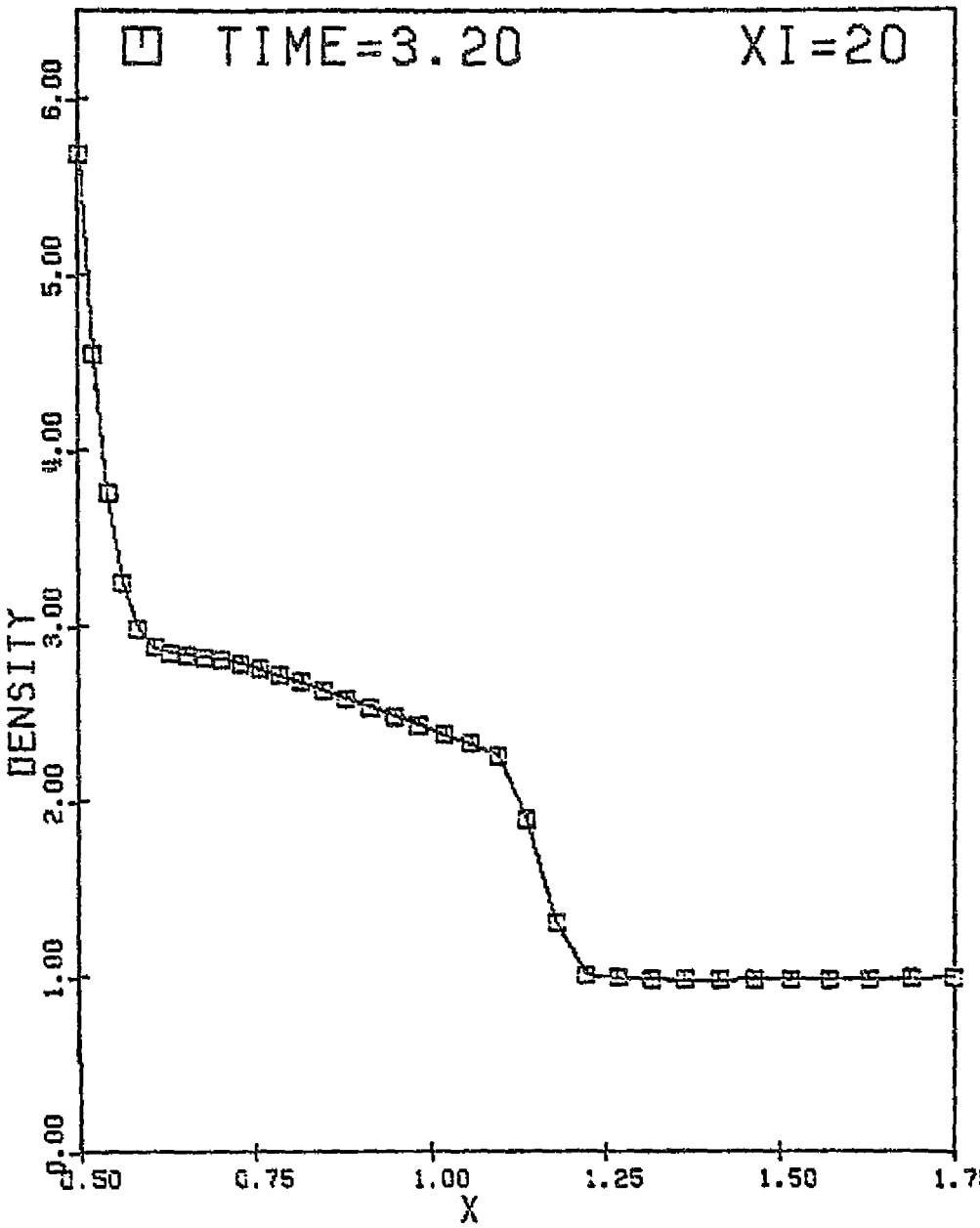

Figure 11. Density Variation Across the Shock on Stagnation Line.

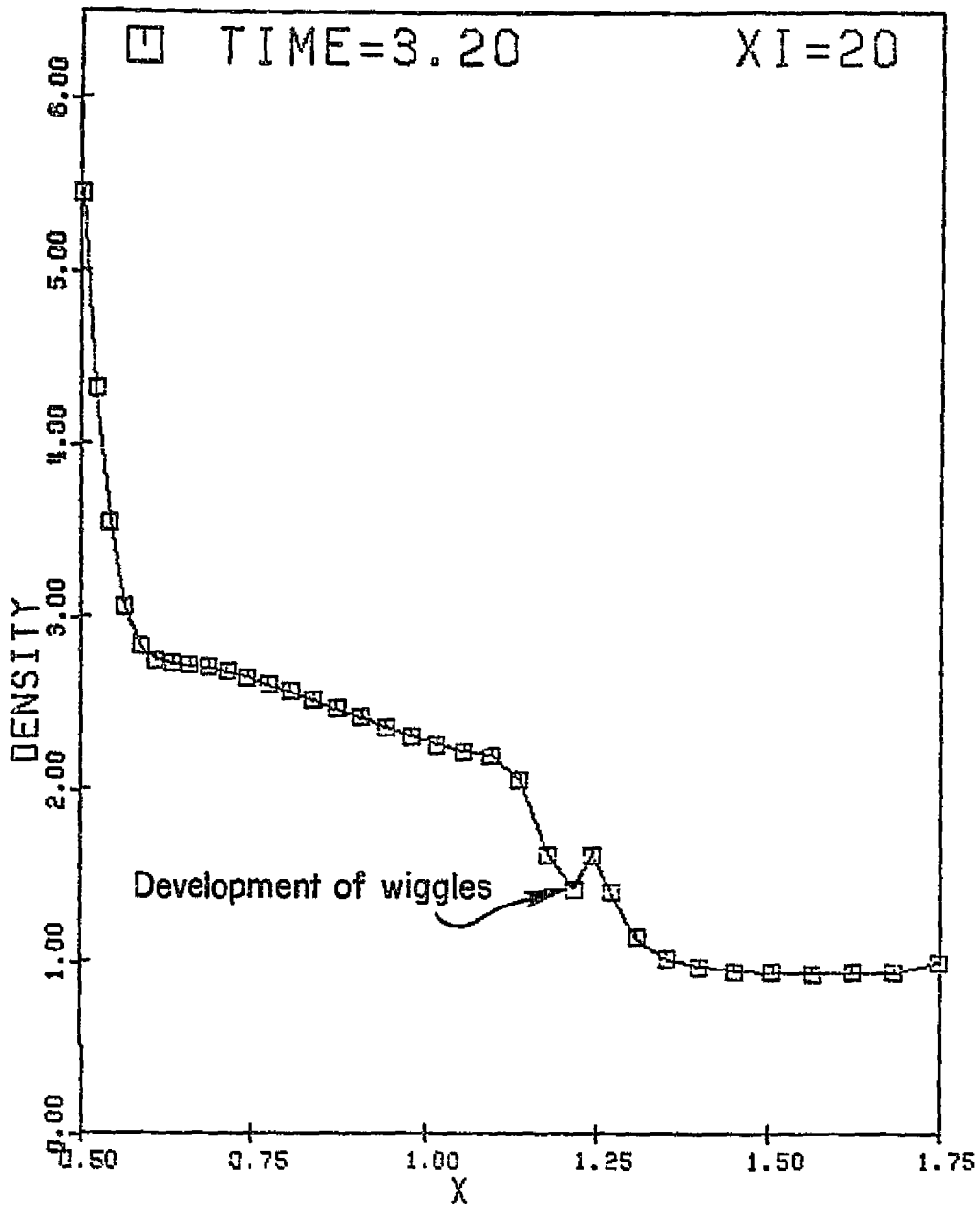

Figure 12. Density Variation Across the Shock for Field with Mesh Refinement.

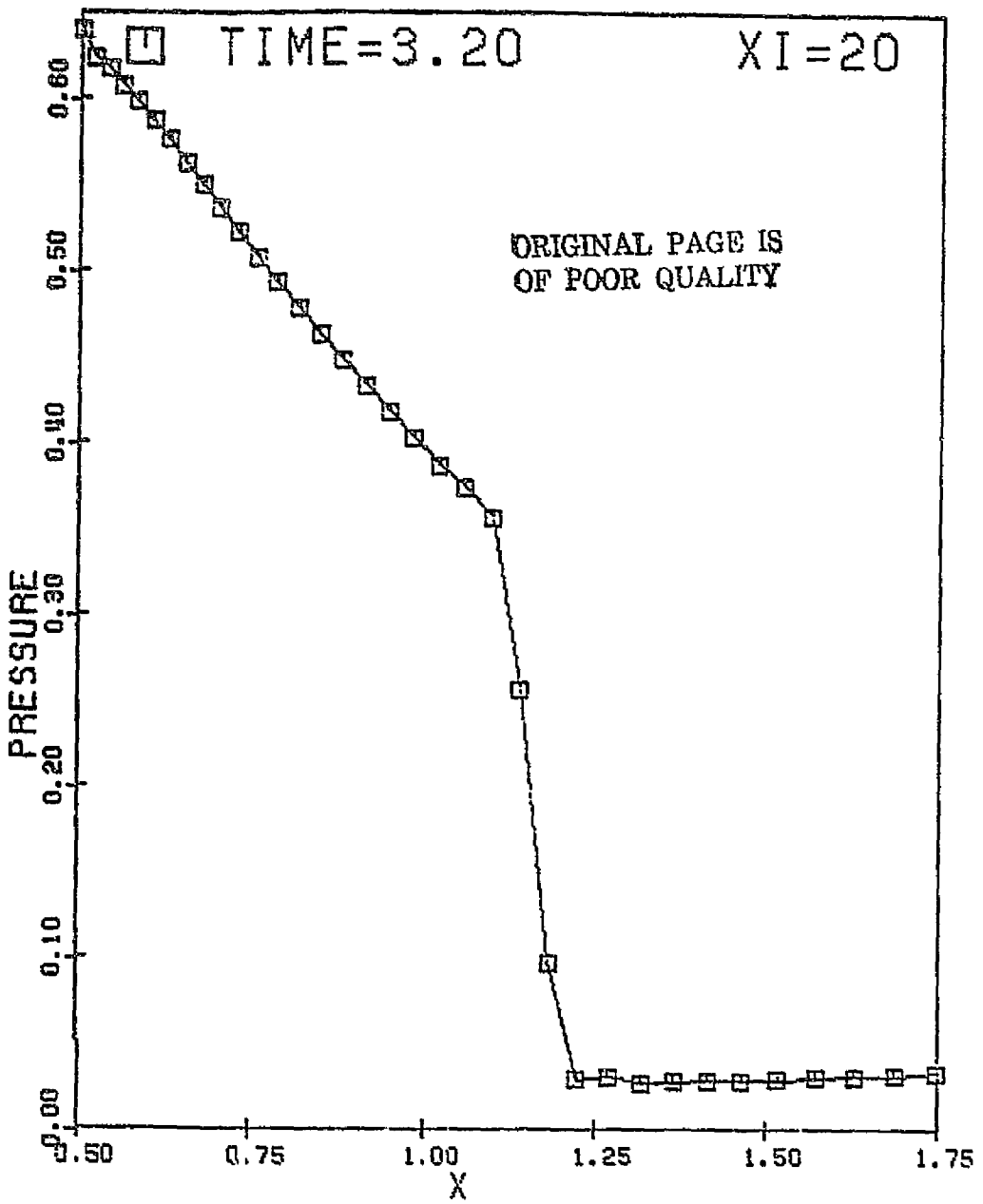

Figure 13. Pressure Variation Across the Shock on Stagnation Line.

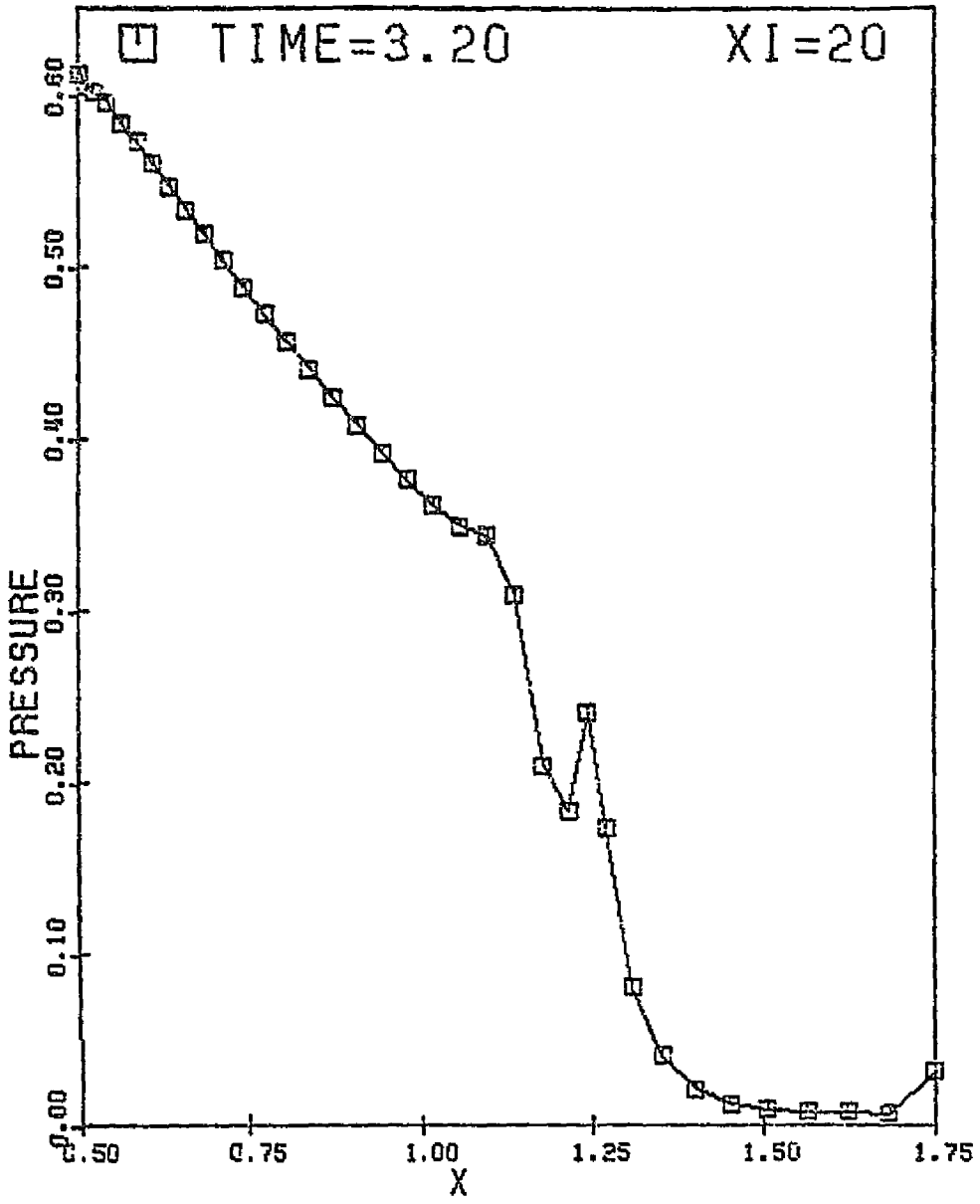

Figure 14. Pressure Variation Across the Shock for Field with Mesh Refinement.

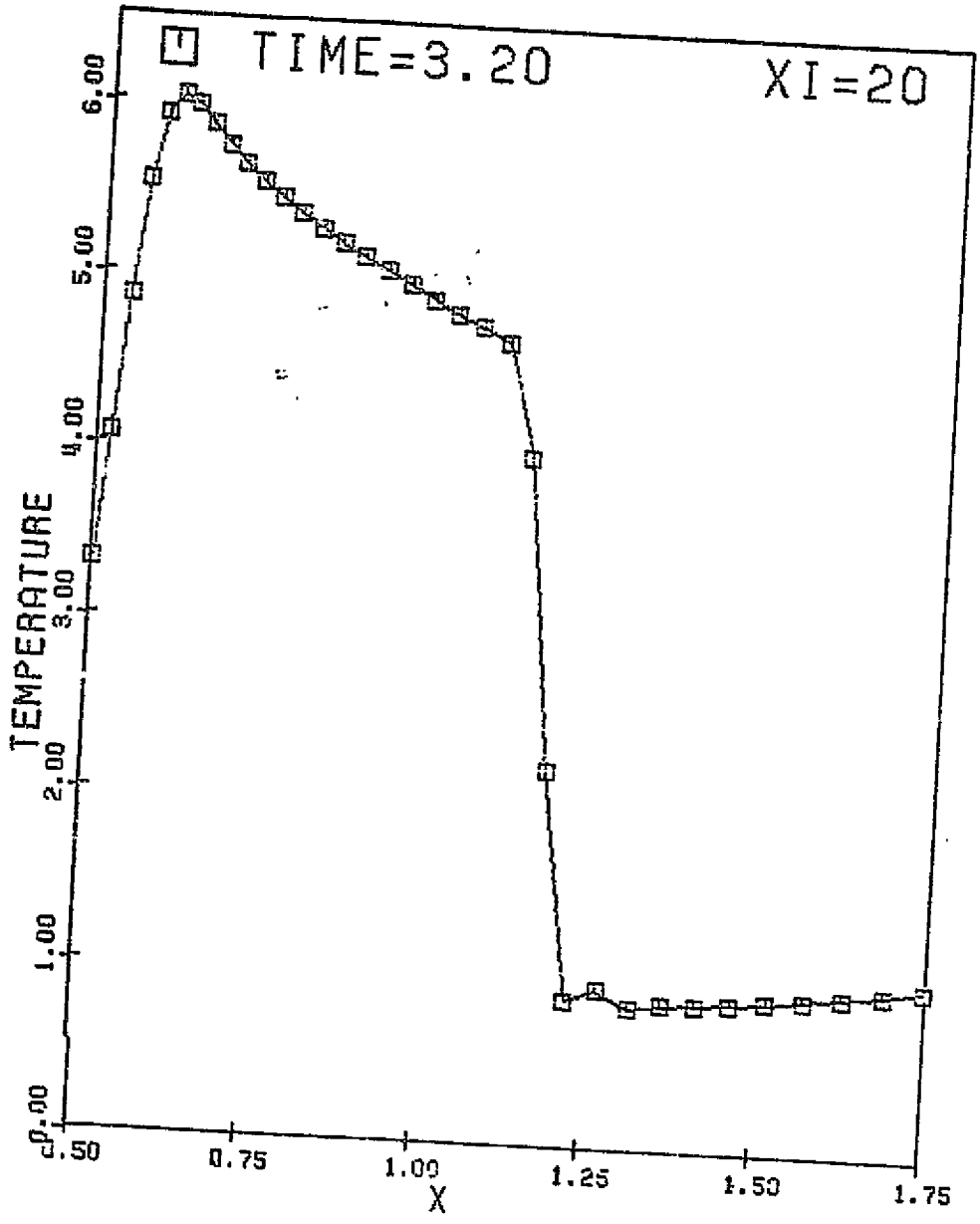

Figure 15. Temperature Variation Across the Shock on Stagnation Line.

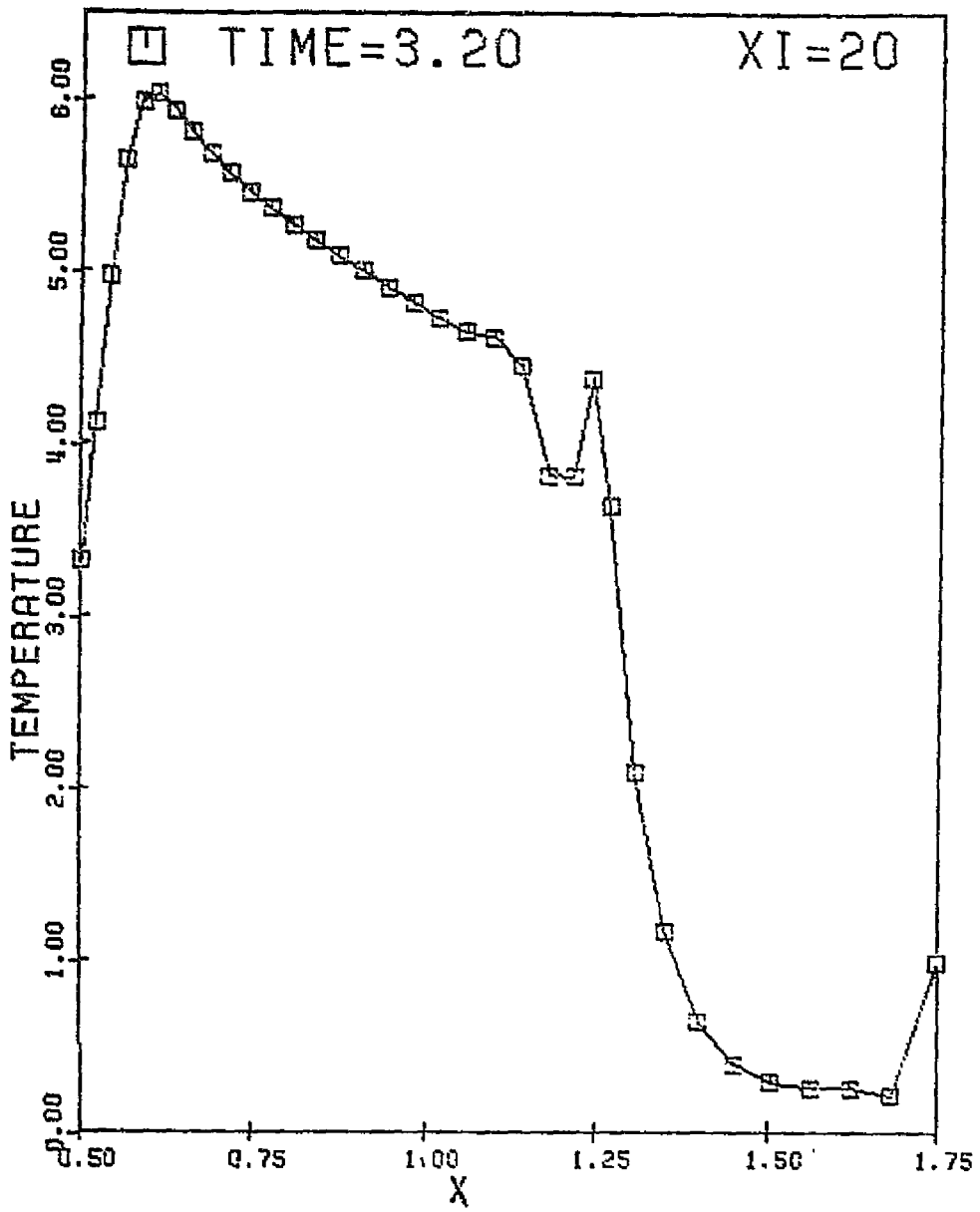

Figure 16. Temperature Variation Across the Shock for Field with Mesh Refinement.

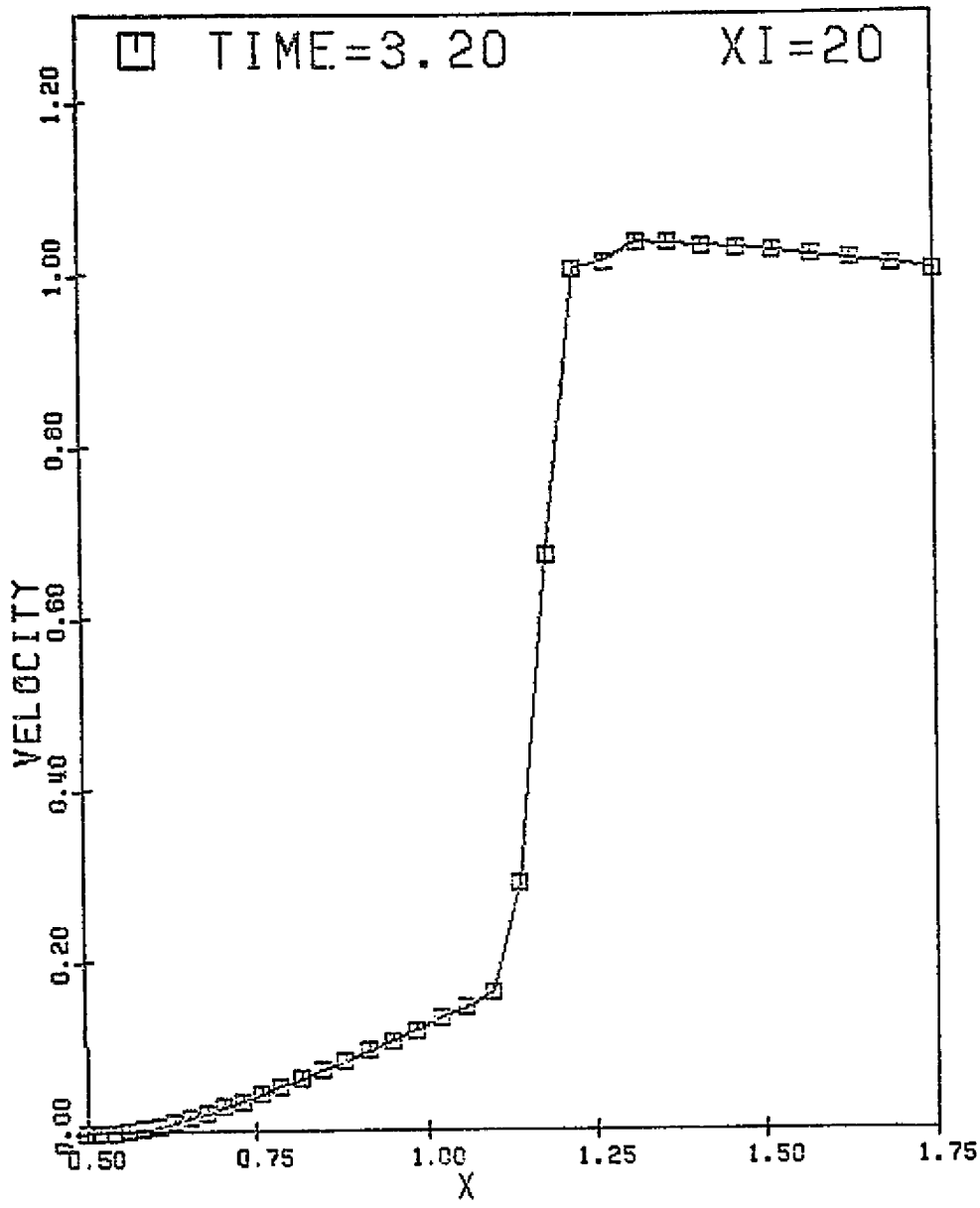

Figure 17. Velocity Variation Across the Shock on Stagnation Line.

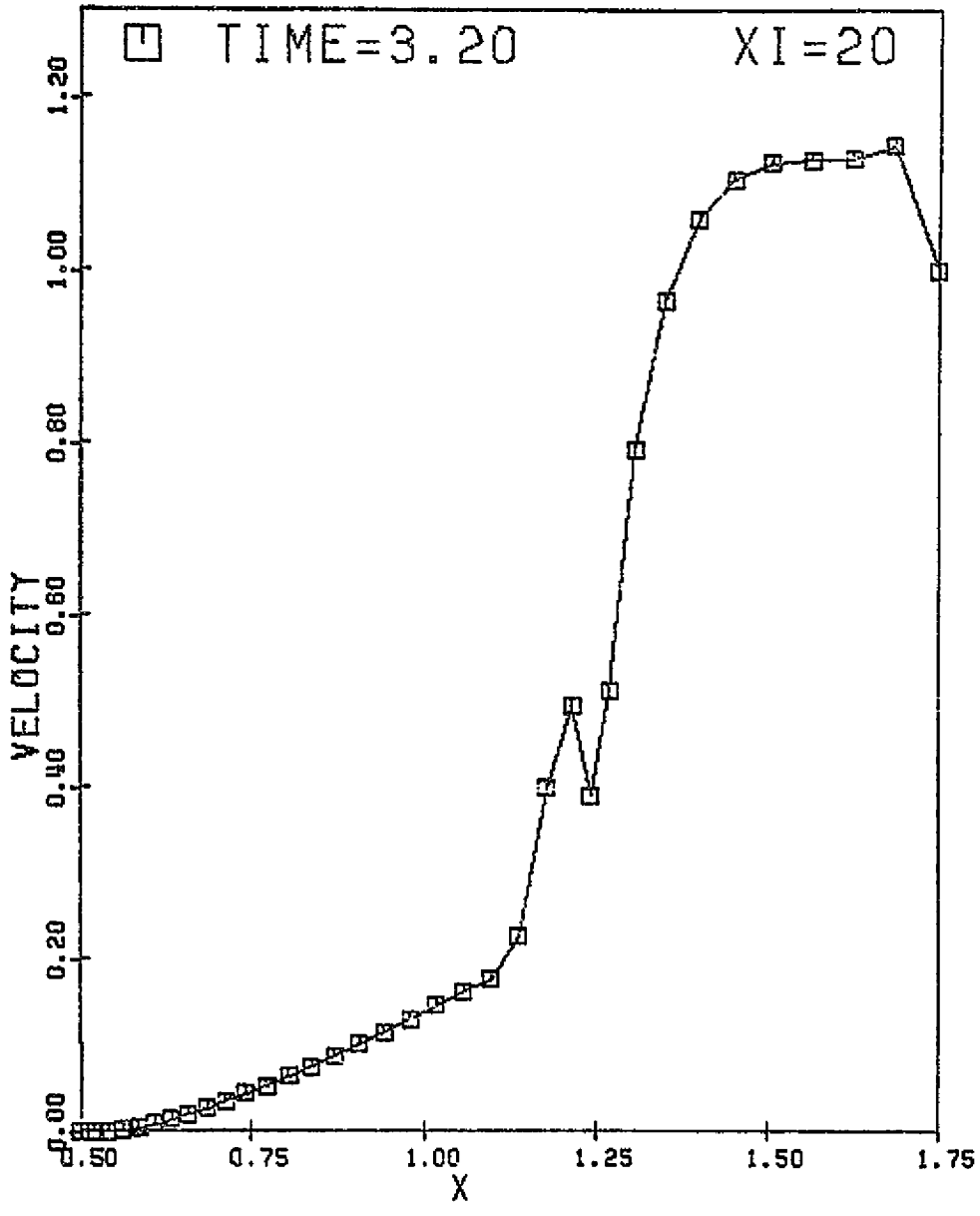

Figure 18. Velocity Variation Across the Shock for Field with Mesh Refinement.

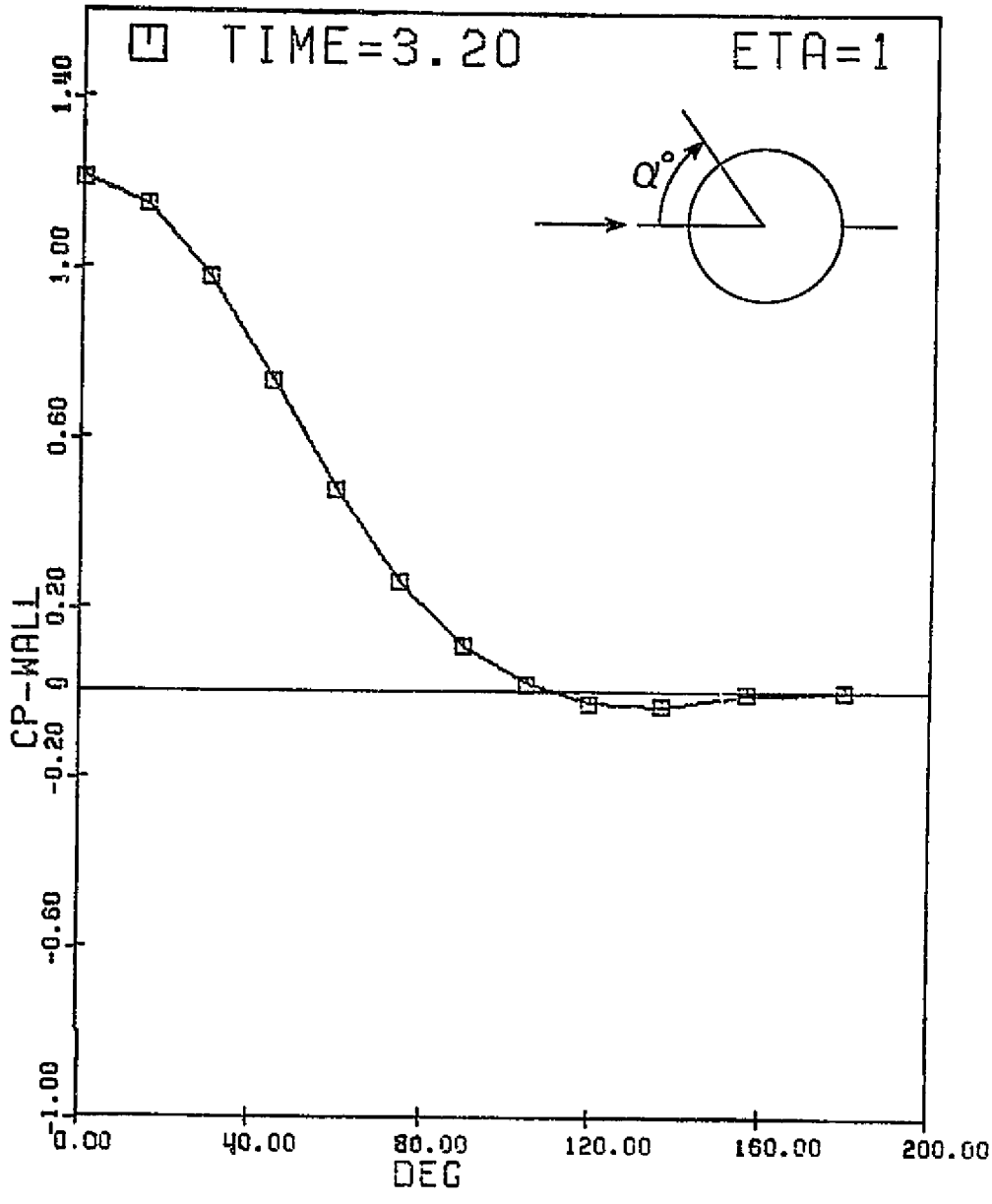

Figure 19. Coefficient of Pressure Distribution on Top of Cylinder.

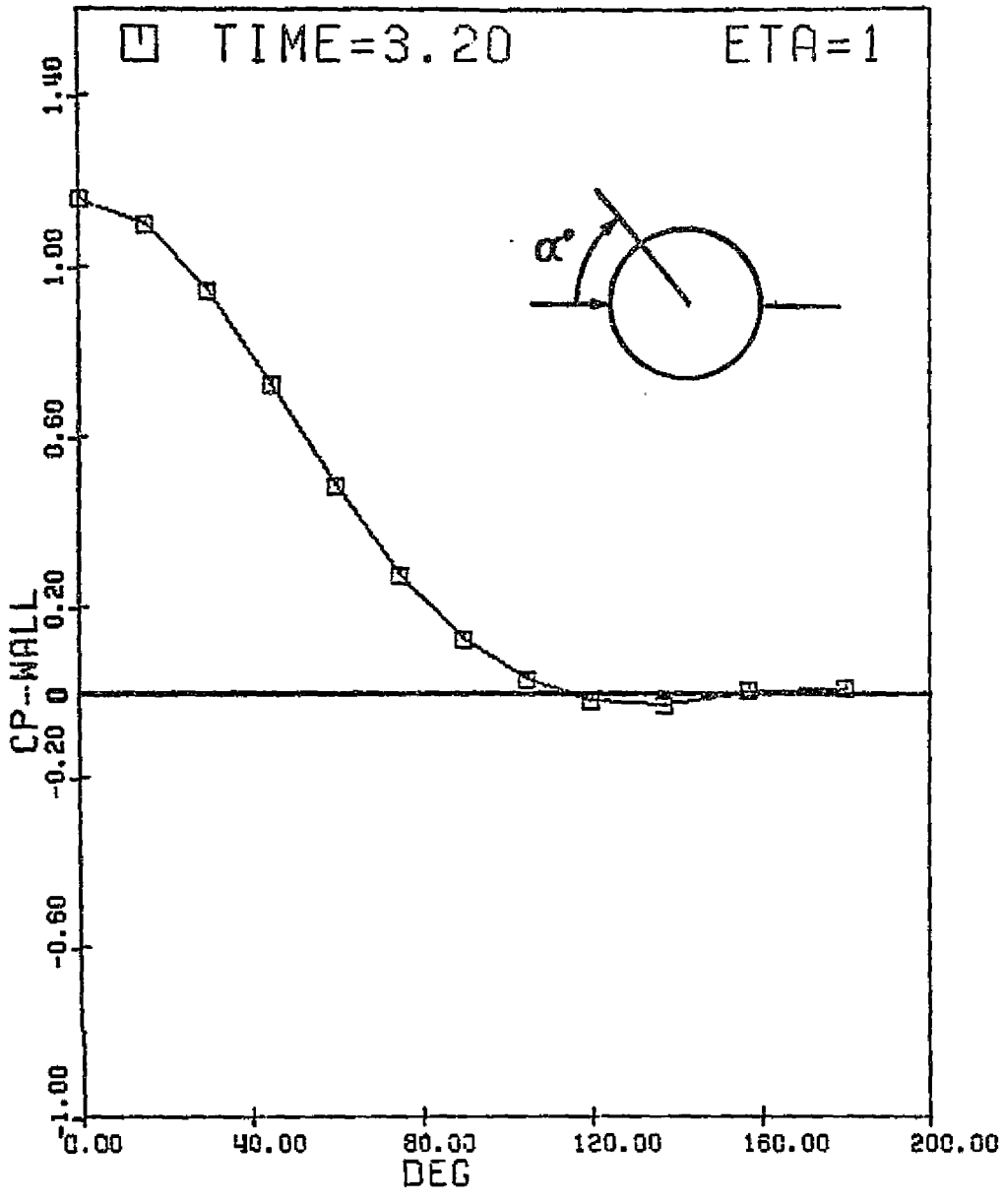

Figure 20. Coefficient of Pressure Distribution for Field with Mesh Refinement.

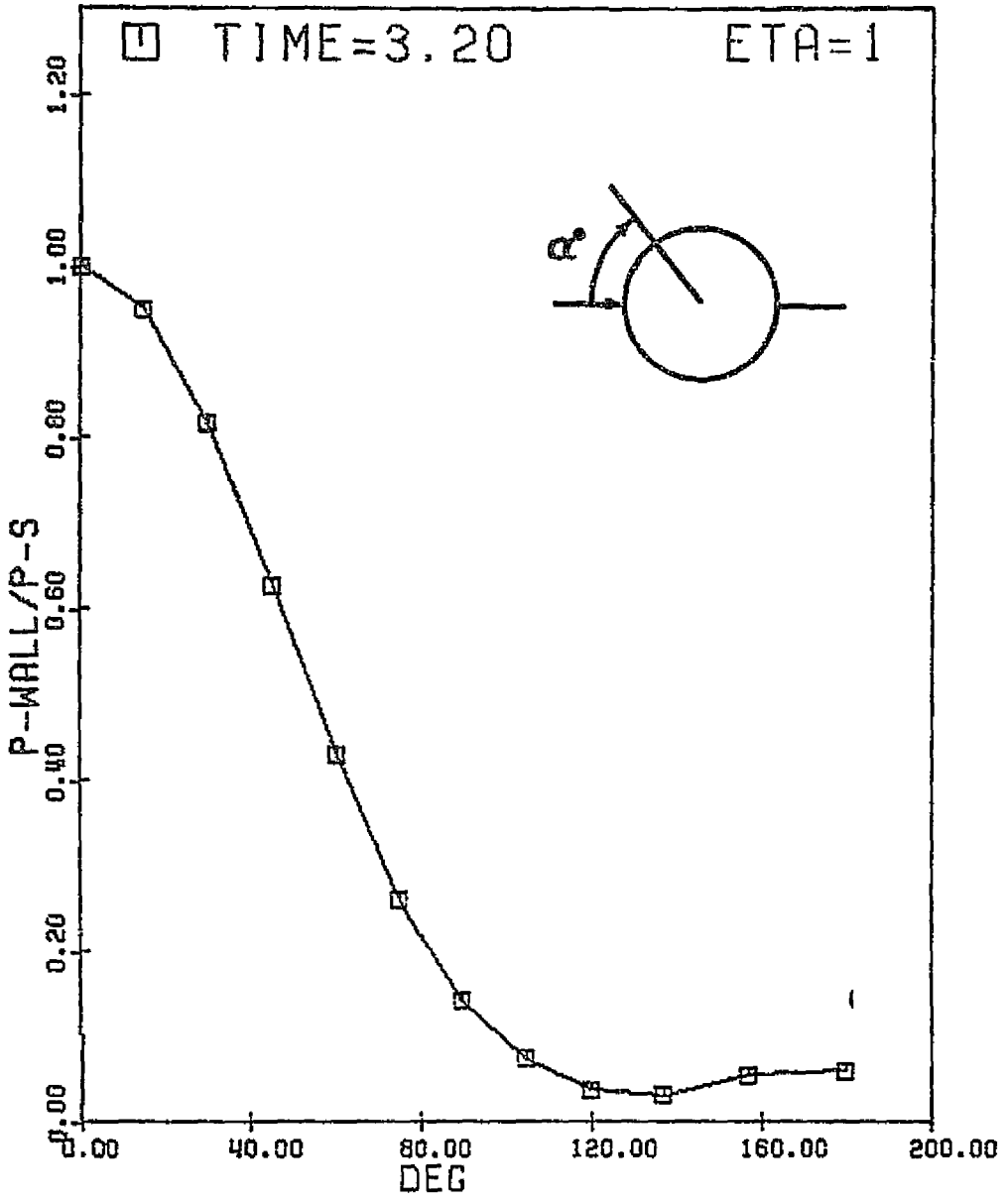

Figure 21. Pressure Distribution on Top of Cylinder.

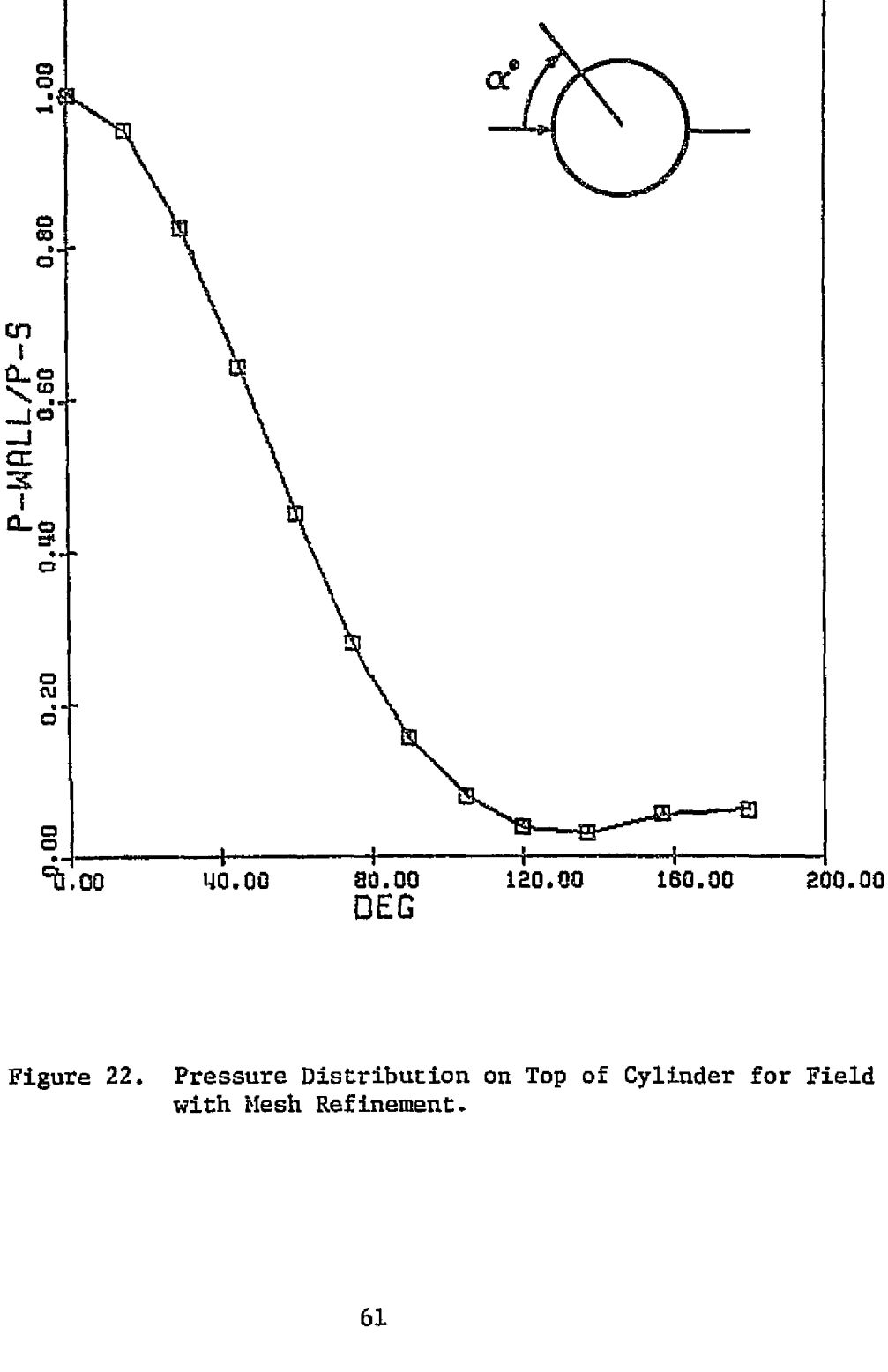

Figure 22. Pressure Distribution on Top of Cylinder for Field with Mesh Refinement.

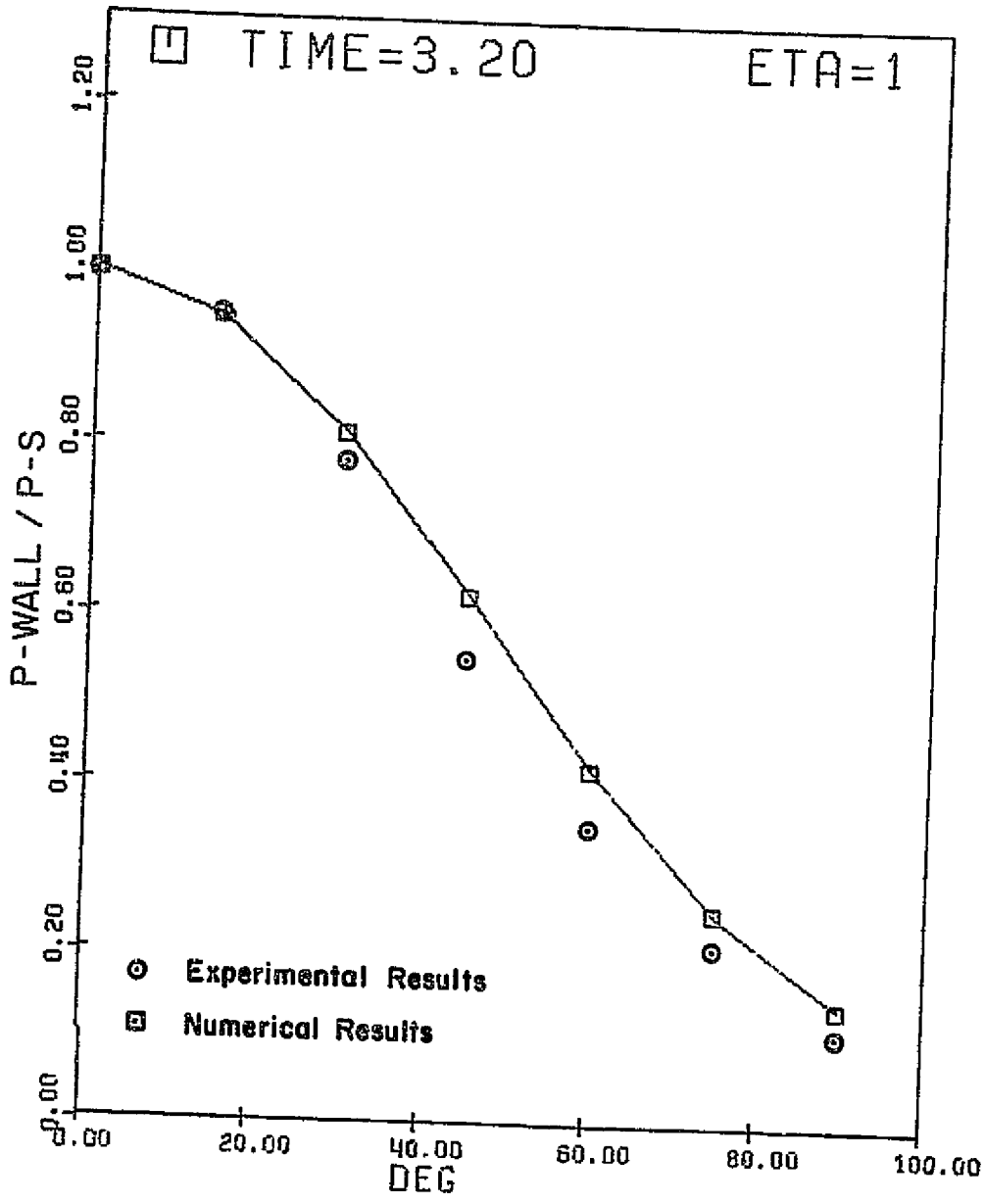

Figure 23. Comparison of Pressure Distribution with Experimental Results.

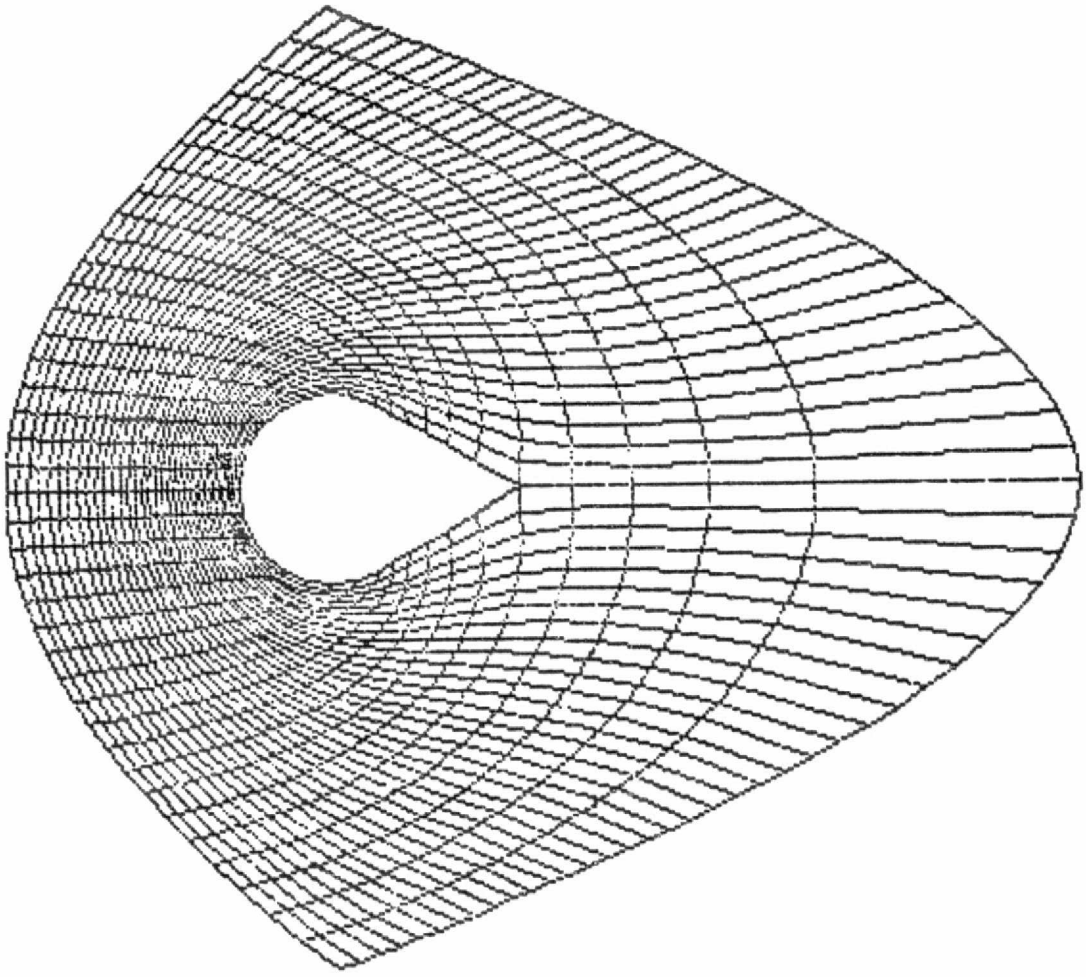

Figure 24. Computational Domain for a Cylinder with a Fairing.

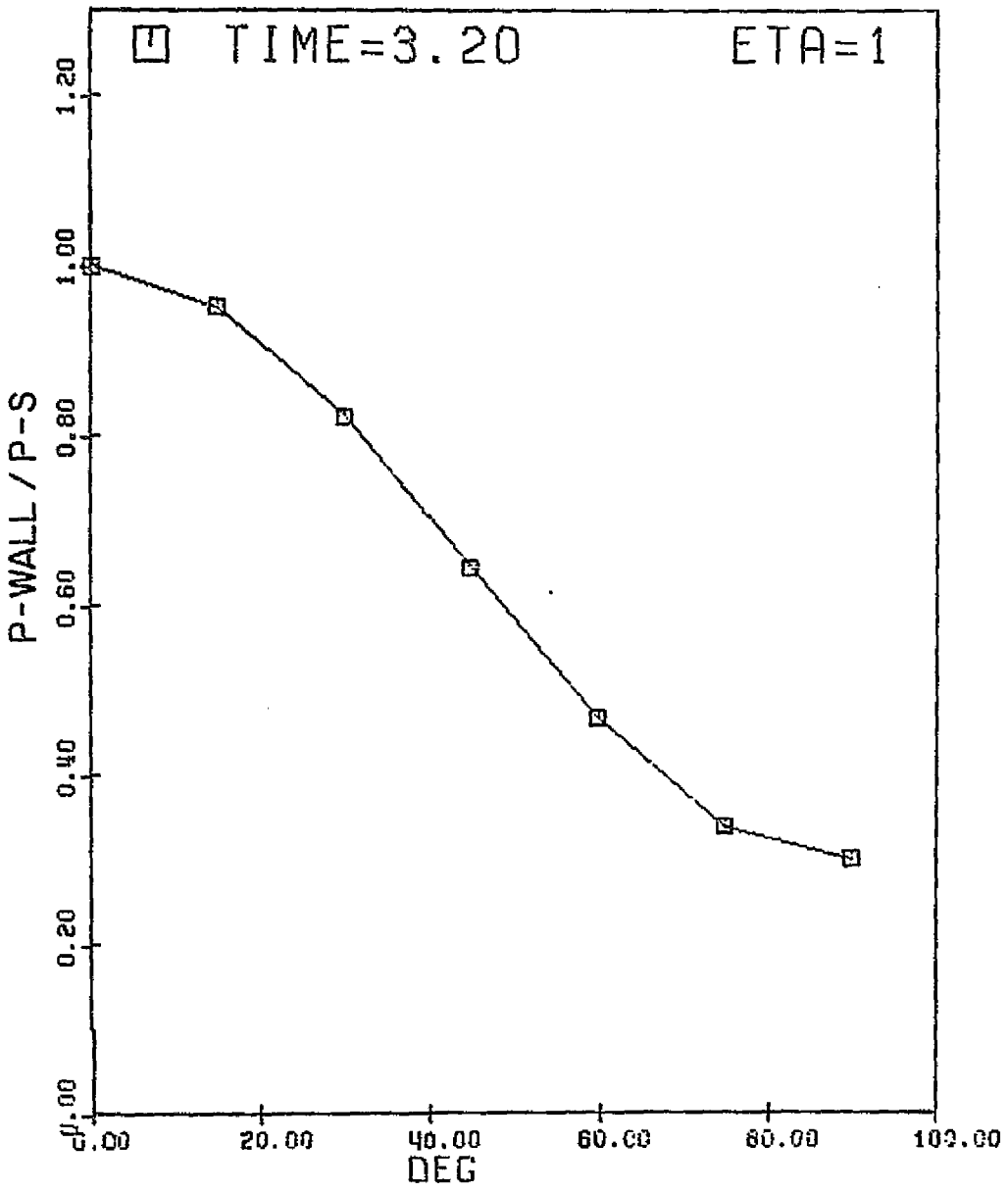

Figure 25. Pressure Distribution on Top of Cylinder with a Fairing.

APPENDIX A

This Appendix summarizes the basic rules of tensor calculus, [16] used in transforming Eqs. (3.1) - (3.3), and the expanded form of the pertinent terms which appear in Eqs. (3.17) - (3.20). In all the formulae given below, repeated indices imply summation.

Lex x_i be the Cartesian coordinates and ξ^i the general curvilinear coordinates. Then the metric coefficients are

$$g_{ij} = \frac{\partial x_k}{\partial \xi^i} \frac{\partial x_k}{\partial \xi^j} \tag{A-1}$$

$$g^{ij} = \frac{\partial \xi^i}{\partial x_k} \frac{\partial \xi^j}{\partial x_k} \tag{A-2}$$

$$g^{ik} g_{jk} = \delta^i_j \tag{A-3}$$

$$g = \det\ (g_{ij}) \tag{A-4}$$

$$J = \sqrt{g} = \frac{\partial (x_1, x_2, x_3)}{\partial (\xi^1, \xi^2, \xi^3)} \tag{A-5}$$

The element of length ds is given by

$$\begin{aligned} (ds)^2 &= \delta_{ij}\, dx_i\, dx_j \\ &= g_{ij}\, d\xi^i\, d\xi^j \end{aligned} \tag{A-6}$$

Based on the above definitions, we collect other formulae from tensor calculus.

Christoffel symbols:

$$\Gamma^i_{jk} = \frac{1}{2}\, g^{i\ell}\, \left(\frac{\partial g_{\ell j}}{\partial x^k} + \frac{\partial g_{\ell k}}{\partial \xi^j} - \frac{\partial g_{jk}}{\partial \xi^\ell}\right) \tag{A-7}$$

which is symmetric in j,k. Contracting the i and j indices, we have

$$\Gamma^k_{kr} = \frac{1}{2g} \frac{\partial g}{\partial \xi^r} \tag{A-8}$$

Covariant Derivative:

$$v^i_{,k} = \frac{\partial v^i}{\partial \xi^k} + \Gamma^i_{kr} \, v^r \tag{A-9}$$

Divergence of a Vector:

$$\text{div } \underline{v} = \frac{1}{\sqrt{g}} \frac{\partial}{\partial \xi^i} (\sqrt{g} \, v^i) \tag{A-10}$$

Divergence of a Tensor yielding Contravariant Components:

$$(\text{div } \bar{\tau})^i = \frac{1}{\sqrt{g}} \frac{\partial}{\partial \xi^k} (\sqrt{g} \, \tau^{ik}) + \Gamma^i_{rs} \, \tau^{rs} \tag{A-11}$$

Laplacian of a Scalar ϕ:

$$\nabla^2 \phi = \frac{1}{\sqrt{g}} \frac{\partial}{\partial \xi^i} (\sqrt{g} \, g^{ik} \frac{\partial \phi}{\partial \xi^k}) \tag{A-12}$$

The transformation of Eqs. (3.1) - (3.3) is now direct. Using contravariant components, Eq. (3.1) becomes

$$\frac{\partial \rho}{\partial t} + \frac{1}{\sqrt{g}} \frac{\partial}{\partial \xi^i} (\rho \sqrt{g} \, v^i) = 0 \tag{A-13}$$

Equation (3.2) becomes

$$\frac{\partial}{\partial t} (\rho v^i) + \frac{1}{\sqrt{g}} \frac{\partial}{\partial \xi^k} (\sqrt{g} \, \tau^{ik}) + \Gamma^i_{rs} \, \tau^{rs} = 0 \tag{A-14}$$

where i = 1,2 for two dimensions.

Equation (3.3) becomes

$$\frac{\partial \Psi}{\partial t} + \frac{1}{\sqrt{g}} \frac{\partial}{\partial \xi^i} (\rho \sqrt{g} \, b^i) = 0 \tag{A-15}$$

The expanded form of these equations are Eqs. (3.11) - (3.13).

The terms appearing in Eqs. (3.17) - (3.20) are

$$\theta = \frac{1}{g}\left(g_{12}\frac{\partial P}{\partial \eta} - g_{22}\frac{\partial P}{\partial \xi}\right) + \frac{P}{g}\left\{g_{22}\left(\Gamma^1_{11} + \Gamma^2_{12}\right)\right.$$

$$\left. - g_{12}\left(\Gamma^1_{12} + \Gamma^2_{22}\right)\right\} + \frac{\varepsilon}{\sqrt{g}}\left(g_{22}\frac{\partial K}{\partial \xi} - g_{12}\frac{\partial K}{\partial \eta}\right)$$

$$+ \varepsilon\left(\frac{\partial D^{11}}{\partial \xi} + \frac{\partial D^{12}}{\partial \eta} + \Gamma^1_{11}D^{11} + 2\Gamma^1_{12}D^{12} + \Gamma^1_{22}D^{22}\right) \qquad \text{(A-16)}$$

$$\phi = \frac{1}{g}\left(g_{12}\frac{\partial P}{\partial \xi} - g_{11}\frac{\partial P}{\partial \eta}\right) + \frac{P}{g}\left\{g_{11}\left(\Gamma^1_{12} + \Gamma^2_{22}\right)\right.$$

$$\left. - g_{12}\left(\Gamma^1_{11} + \Gamma^2_{12}\right)\right\} + \frac{\varepsilon}{\sqrt{g}}\left(g_{11}\frac{\partial K}{\partial \eta} - g_{12}\frac{\partial K}{\partial \xi}\right)$$

$$+ \varepsilon\left(\frac{\partial D^{12}}{\partial \xi} + \frac{\partial D^{22}}{\partial \eta} + \Gamma^2_{11}D^{11} + 2\Gamma^2_{12}D^{12} + \Gamma^2_{22}D^{22}\right) \qquad \text{(A-17)}$$

$$\psi = \varepsilon\left\{\frac{\partial}{\partial \xi}\left(\sqrt{g}\,v^1\right) + \frac{\partial}{\partial \eta}\left(\sqrt{g}\,v^2\right)\right.$$

$$+ \alpha_o\frac{\partial}{\partial \xi}\left\{\frac{\mu}{\sqrt{g}}\left(g_{22}\frac{\partial T}{\partial \xi} - g_{12}\frac{\partial T}{\partial \eta}\right)\right\}$$

$$\left. + \alpha_o\frac{\partial}{\partial \eta}\left\{\frac{\mu}{\sqrt{g}}\left(g_{11}\frac{\partial T}{\partial \eta} - g_{12}\frac{\partial T}{\partial \xi}\right)\right\}\right\} \qquad \text{(A-18)}$$

Defining

$$G_{ij} = g_{ij}/\sqrt{g} \qquad \text{(A-19)}$$

the terms D^{11}, D^{12}, . . . , v^1 v^2, etc., are

$$D^{11} = 2\mu[G_{22}\,u_\xi - G_{12}\,u_\eta + (G_{22}\,\Gamma^1_{11} - G_{12}\,\Gamma^1_{12})u$$

$$+ (G_{22}\,\Gamma^1_{12} - G_{12}\,\Gamma^1_{22})v] \qquad \text{(A-20)}$$

$$D^{12} = \mu[(G_{11}\, u_\eta + G_{22}\, v_\xi) - G_{12}\,(u_\xi + v_\eta)$$

$$+ \{G_{22}\,\Gamma^2_{11} + G_{11}\,\Gamma^1_{12} - G_{12}\,(\Gamma^1_{11} + \Gamma^2_{12})\}u$$

$$+ \{G_{22}\,\Gamma^2_{12} + G_{11}\,\Gamma^1_{22} - G_{12}\,(\Gamma^1_{12} + \Gamma^2_{22})\}v] \qquad \text{(A-21)}$$

$$D^{22} = 2\mu[G_{11}\, v_\eta - G_{12}\, v_\xi + (G_{11}\,\Gamma^2_{12} - G_{12}\,\Gamma^2_{11})u$$

$$+ (G_{11}\,\Gamma^2_{22} - G_{12}\,\Gamma^2_{12})v] \qquad \text{(A-22)}$$

$$K = \lambda\,[u_\xi + v_\eta + (\Gamma^1_{11} + \Gamma^2_{12})u + (\Gamma^1_{12} + \Gamma^2_{22})v] \qquad \text{(A-23)}$$

$$\nu^1 = Ku + \mu(G_{11}\,G_{22}\,u + G_{12}\,G_{22}\,v + u)v^1_{,1}$$

$$+ \mu\{G_{12}\,G_{22}\,u + (G_{22})^2 v\}v^2_{,1} - \mu\{G_{11}\,G_{12}\,u + (G_{12})^2 v - v\}v^1_{,2}$$

$$- \mu\{(G_{12})^2 u + G_{11}\,G_{22}\,v\}v^2_{,2} \qquad \text{(A-24)}$$

$$\nu^2 = Kv - \mu\{G_{11}\,G_{12}\,u + (G_{12})^2 v\}v^1_{,1}$$

$$- \mu\{(G_{12})^2 u + G_{12}\,G_{22}\,v - u\}v^2_{,1}$$

$$+ \mu\{(G_{11})^2 u + G_{11}\,G_{12}\,v\}v^1_{,2}$$

$$+ \mu\{G_{11}\,G_{12}\,u + G_{11}\,G_{22}\,v + v\}v^2_{,2} \qquad \text{(A-25)}$$

APPENDIX B

EQUATION FOR NUMERICAL COORDINATE GENERATION

As in Appendix A, we shall denote the Cartesian coordinates as x_i (the index i serving as a label only, having no tensorial significance) and the curvilinear coordiantes either as x^i, or $\bar{x}^i$, or ξ^i.

It was mentioned in Section 2 that we need formulae in which the Cartesian coordinates x_i are treated as dependent variables, while the curvilinear coordinates ξ^i are treated as independent variables. To achieve this goal, we shall use some formulae from general tensor calculus. In all the expressions given below, the repeated indices imply summation.

Formula for the Second Derivative:

Let x^i and $\bar{x}^i$ be two general coordinate systems. The formula for the second derivative [16] is

$$\frac{\partial^2 x^r}{\partial \bar{x}^\ell \partial \bar{x}^m} = \bar{\Gamma}^p_{\ell m} \frac{\partial x^r}{\partial \bar{x}^p} - \Gamma^r_{ij} \frac{\partial x^i}{\partial \bar{x}^\ell} \frac{\partial x^j}{\partial \bar{x}^m} \tag{B-1}$$

where Γ^i_{jk} and $\bar{\Gamma}^i_{jk}$ are the Christoffel symbols in the x^i and $\bar{x}^i$ coordinate systems respectively. (Refer to Eq. (A-7) for definition). Since we are considering the transformation between a Cartesian and a curvilinear system, hence either x^i or $\bar{x}^i$ is a Cartesian system.

If x^r is a Cartesian system, then $\Gamma^r_{ij} \equiv 0$. Writing $x^r = x_r$ and $\bar{x}^i = \xi^i$, we have

$$\frac{\partial^2 x_r}{\partial \xi^\ell \partial \xi^m} = \Gamma^p_{\ell m} \frac{\partial x_r}{\partial \xi^p} \tag{B-2}$$

which is the formula for the second derivative of any Cartesian coordinate with respect to the curvilinear coordinates.

Next, if $\bar{x}^i$ is a Cartesian system, then $\bar{\Gamma}^p_{\ell m} = 0$. Writing $\bar{x}^i = x_i$ and $x^i = \xi^i$, we have

$$\frac{\partial^2 \xi^r}{\partial x_\ell \, \partial x_m} = - \Gamma^r_{ij} \frac{\partial \xi^i}{\partial x_\ell} \frac{\partial \xi^j}{\partial x_m} \tag{B-3}$$

which is the formula for the second derivative of any curvilinear coordinate with respect to the Cartesian coordinates.

The use of Eqs. (B-2) and (B-3) along with the equations

$$\frac{\partial \xi^i}{\partial x_\ell} = g^{ip} \frac{\partial x_\ell}{\partial \xi^p} \tag{B-4}$$

$$\frac{\partial x_r}{\partial \xi^p} \frac{\partial \xi^n}{\partial x_r} = \delta^n_p \tag{B-5}$$

yields a series of useful equations.

Inner multiplication of Eq. (B-2) with $\frac{\partial \xi^n}{\partial x_r}$ and use of Eq. (B-5) yields

$$\Gamma^r_{ij} = \frac{\partial \xi^r}{\partial x_s} \frac{\partial^2 x_s}{\partial \xi^i \, \partial \xi^j} \tag{B-6}$$

Using Eq. (B-4) in (B-7), we have

$$\Gamma^r_{ij} = g^{rt} \frac{\partial x_s}{\partial \xi^t} \frac{\partial^2 x_s}{\partial \xi^i \, \partial \xi^j} \tag{B-7}$$

Introducing Eq. (B-4) in Eq. (B-3), we have

$$\frac{\partial^2 \xi^r}{\partial x_\ell \, \partial x_m} = - \Gamma^r_{ij} \, g^{ip} \, g^{jq} \frac{\partial x_\ell}{\partial \xi^p} \frac{\partial x_m}{\partial \xi^q} \tag{B-8}$$

Another form of (B-8) can be obtained by using (B-7), which is

$$\frac{\partial^2 \xi^r}{\partial x_\ell \, \partial x_m} = - g^{rt} \, g^{ip} \, g^{jq} \frac{\partial^2 x_s}{\partial \xi^i \, \partial \xi^j} \frac{\partial x_s}{\partial \xi^t} \frac{\partial x_\ell}{\partial \xi^p} \frac{\partial x_m}{\partial \xi^q} \tag{B-9}$$

It must be noted that the right hand sides of Eqs. (B-7) - (B-9) have differentiations with respect to ξ^i, as desired.

Laplacian:

Setting $\ell = m$ in Eq. (B-9), using Eqs. (A-1) and (A-3), and summing over the index m, we get

$$\nabla^2 \xi^r = - g^{rt} g^{ij} \frac{\partial x_s}{\partial \xi^t} \frac{\partial^2 x_s}{\partial \xi^i \partial \xi^j} \tag{B-10}$$

In two dimensions, writing

$$\xi^1 = \xi, \ \xi^2 = \eta, \ x_1 = x, \ x_2 = y \tag{B-11}$$

and using

$$g^{11} = g_{22}/g, \ g^{12} = - g_{12}/g, \ g^{22} = g_{11}/g \tag{B-12}$$

(which are a consequence of Eq. (A-3)), we have

$$\nabla^2 \xi = [(g_{22} y_{\xi\xi} - 2g_{12} y_{\xi\eta} + g_{11} y_{\eta\eta}) x_\eta - (g_{22} x_{\xi\xi} - 2g_{12} x_{\xi\eta} + g_{11} x_{\eta\eta}) y_\eta]/g^{3/2} \tag{B-13}$$

$$\nabla^2 \eta = [(g_{22} x_{\xi\xi} - 2g_{12} x_{\xi\eta} + g_{11} x_{\eta\eta}) y_\xi - (g_{22} y_{\xi\xi} - 2g_{12} y_{\xi\eta} + g_{11} y_{\eta\eta}) x_\xi]/g^{3/2} \tag{B-14}$$

where

$$g = g_{11} g_{22} - (g_{12})^2 \tag{B-15}$$

Similarly, using (B-3) and (B-4), we easily obtain

$$\xi^r_{xy} = [\Gamma^r_{11} x_\eta y_\eta - \Gamma^r_{12} (x_\xi y_\eta + x_\eta y_\xi) + \Gamma^r_{22} x_\xi y_\xi]/g \tag{B-16}$$

where $\xi^1 = \xi$ and $\xi^2 = \eta$.

The Laplacian of a scalar function $f(\xi^i)$ is obtained as div (grad f),

$$\nabla^2 f = \frac{1}{\sqrt{g}} \frac{\partial}{\partial \xi^i} (\sqrt{g} \, g^{ik} \frac{\partial f}{\partial \xi^k}) \tag{B-17}$$

which in two dimensions has the form

$$\nabla^2 f = [(g_{22}\, f_{\xi\xi} - 2g_{12}\, f_{\xi\eta} + g_{11}\, f_{\eta\eta})$$

$$+ (2g_{12}\, \Gamma^1_{12} - g_{22}\, \Gamma^1_{11} - g_{11}\, \Gamma^1_{22}) f_\xi$$

$$+ (2g_{12}\, \Gamma^2_{12} - g_{22}\, \Gamma^2_{11} - g_{11}\, \Gamma^2_{22}) f_\eta]/g \qquad \text{(B-18)}$$

Unit Tangent and Normal Vectors:

In the generation of coordinates we have taken clockwise traverse along the body contour as positive. Denoting the unit tangent and normal vectors as $\underset{\sim}{t}$ and $\underset{\sim}{n}$ respectively, and $\underset{\sim}{k}$ the constant unit vector normal to the plane of the curve, the vectors ($\underset{\sim}{t}$, $\underset{\sim}{n}$, $\underset{\sim}{k}$) are assumed to form a right-handed system. The unit tangent and normal vectors for the ξ = const. and η = const. curves are

$$(\underset{\sim}{t})_{\xi = \text{const.}} = -\frac{1}{\sqrt{g_{22}}} (\underset{\sim}{i} x_\eta + \underset{\sim}{j} y_\eta) \qquad \text{(B-19)}$$

$$(\underset{\sim}{t})_{\eta = \text{const.}} = \frac{1}{\sqrt{g_{11}}} (\underset{\sim}{i} x_\xi + \underset{\sim}{j} y_\xi) \qquad \text{(B-20)}$$

$$(\underset{\sim}{n})_{\xi = \text{const.}} = \frac{1}{\sqrt{g_{22}}} (\underset{\sim}{i} y_\eta - \underset{\sim}{j} x_\eta) \qquad \text{(B-21)}$$

$$(\underset{\sim}{n})_{\eta = \text{const.}} = \frac{1}{\sqrt{g_{11}}} (-\underset{\sim}{i} y_\xi + \underset{\sim}{j} x_\xi) \qquad \text{(B-22)}$$

where $\underset{\sim}{i}$ and $\underset{\sim}{j}$ are unit vectors along x and y respectively. The resolved parts of the velocity vector along the curves ξ = const. and η = const. are

$$(\underset{\sim}{v}\cdot\underset{\sim}{t})_{\xi = \text{const.}} = -\frac{1}{\sqrt{g_{22}}} (u g_{12} + v g_{22}) \qquad \text{(B-23)}$$

$$(\underset{\sim}{v}\cdot\underset{\sim}{t})_{\eta = \text{const.}} = \frac{1}{\sqrt{g_{11}}}\,(ug_{11} + vg_{12}) \tag{B-24}$$

$$(\underset{\sim}{v}\cdot\underset{\sim}{n})_{\xi = \text{const.}} = \sqrt{\frac{g}{g_{22}}}\,u \tag{B-25}$$

$$(\underset{\sim}{v}\cdot\underset{\sim}{n})_{\eta = \text{const.}} = \sqrt{\frac{g}{g_{11}}}\,v \tag{B-26}$$

where u and v are the contravariant components of the velocity vector $\underset{\sim}{v}$, which are related to the Cartesian components through Eq. (3.26).

APPENDIX C

FINITE-DIFFERENCE APPROXIMATION OF THE N-S EQUATIONS

This Appendix gives the details of the discretization of the N-S Equations, Eq. (4.1), by a fully implicit difference approximation. The time derivatives are approximated by first-order backward differences, while the spatial derivatives are approximated by central differences. The resulting system of finite-difference equations are solved by the S.O.R. method. In what follows below the quantities at the previous time step are denoted by an overhead bar. Also $\Delta\xi$ and $\Delta\eta$ do not occur in these equations as they both equal 1.

Finite-differencing of equation (3.17):

$$(\sigma_{ij})^* = \bar{\sigma}_{i,J} - (\Delta t/2)\,[(A_{i+1,J} - A_{i-1,j}) + (B_{i,J+1} - B_{i,J-1})] \qquad \text{(C-1)}$$

In the S.O.R. scheme (C-1) is used as follows:

$$\sigma_{i,J} = (1-\omega)\,\sigma_{i,J}{}^{p} + \omega(\sigma_{i,J})^* \qquad \text{(C-2)}$$

In Equation (C-2) the superscript p denotes that the quantity is from the previous iteration. The second term on the R.H.S. of Equation (C-2) marked by an asterik is a provisional term defined by Equation (C-1), which is recovered from (C-2) for $\omega = 1$. $\omega = 0$ indicates that no progress is being made in iterative convergence, which is a trivial case.

The finite-differencing of Equations (3-18) through (3.20) are carried out in a similar fashion:

$$(A_{i,J})^* = \overline{A}_{i,J} - (\Delta t/2)\ [(H_{i+1,j} - H_{i-1,J}) + (N_{i,J+1} - N_{i,J-1})] - \Delta t\ [\Gamma^1_{11}H + 2\Gamma^1_{12}N + \Gamma^1_{22}M - \theta]_{i,J} \qquad (C\text{-}3)$$

$$A_{i,J} = (1-\omega)\ A_{i,j}{}^{p} + \omega(A_{i,J})^* \qquad (C\text{-}4)$$

$$(B_{i,J})^* = \overline{B}_{i,J} - (\Delta t/2)\ [(N_{i+1,J} - N_{i-1,J}) + (M_{i,J+1} - M_{i,J-1})] - \Delta t[\Gamma^2_{11}H + 2\Gamma^2_{12}N + \Gamma^2_{22}M - \phi]_{i,j} \qquad (C\text{-}5)$$

$$B_{i,J} = (1-\omega)\ B_{i,j}{}^{p} + \omega(B_{i,J})^* \qquad (C\text{-}6)$$

$$(E_{i,J})^* = \overline{E}_{i,j} - (\Delta t/2)\ [(Q_{i+1,J} - Q_{9-1,J}) + (R_{i,J+1} - R_{i,J-1})] - \Delta t\Psi_{i,J} \qquad (C\text{-}7)$$

$$E_{i,J} = (1-\omega)\ E_{i,J}{}^{p} + \omega(E_{i,J})^* \qquad (C\text{-}8)$$

The terms θ, ϕ and Ψ that occur in Equations (C-3), (C-5) and (C-7) are defined by Equations (A-16), (A-17) and (A-18), repectively. The finite-differencing of these equations is carried out next.

Certain combinations of Christoffels and other terms that occur in groups frequently have been abbreviated as follows:

$$DA = [(G_{22}(\Gamma^1_{11} + \Gamma^2_{12}) - G_{12}(\Gamma^1_{12} + \Gamma^2_{22}))/\sqrt{g}]_{i,j}$$

$$DB = [G_{22}\Gamma^1_{11} - G_{12}\Gamma^1_{12}]_{i,j}$$

$$DC = [G_{22}\Gamma^1_{11} - G_{12}\Gamma^1_{12}]_{i-1,j}$$

$$DD = [G_{22}\Gamma^1_{12} - G_{12}\Gamma^1_{22}]_{i+1,j}$$

$$DE = [G_{22}\Gamma^1_{12} - G_{12}\Gamma^1_{22}]_{i-1,j}$$

$$DF = [G_{22}\Gamma^2_{11} + G_{11}\Gamma^1_{12} - G_{12}(\Gamma^1_{11} + \Gamma^2_{12})]_{i,j}$$

$$DG = [G_{22}\Gamma^2_{11} + G_{11}\Gamma^1_{12} - G_{12}(\Gamma^1_{11} + \Gamma^2_{12})]_{i,j-1}$$

$$DH = [G_{22}\Gamma^2_{12} + G_{11}\Gamma^1_{22} - G_{12}(\Gamma^1_{12} + \Gamma^2_{22})]_{i,j+1}$$

$$DI = [G_{22}\Gamma^2_{12} + G_{11}\Gamma^1_{22} - G_{12}(\Gamma^1_{12} + \Gamma^2_{22})]_{i,j-1}$$

$$DJ = [G_{11}\Gamma^2_{12} - G_{12}\Gamma^2_{11}]_{i,j}$$

$$DK = [G_{22}\Gamma^1_{12} - G_{12}\Gamma^1_{22}]_{i,j}$$

$$DL = [G_{22}\Gamma^2_{12} + G_{11}\Gamma^1_{22} - G_{12}(\Gamma^1_{12} + \Gamma^2_{22})]_{i,j}$$

$$DM = [G_{11}\Gamma^2_{22} - G_{12}\Gamma^2_{12}]_{i,j}$$

$$DN = [G_{12}(\Gamma^1_{11} + \Gamma^2_{12})/\sqrt{g}]_{i,j}$$

$$DO = [G_{22}\Gamma^2_{11} + G_{11}\Gamma_{12} - G_{12}(\Gamma^1_{11} + \Gamma^2_{12})]_{i-1,j}$$

$$DP = [G_{22}\Gamma^2_{12} + G_{11}\Gamma^1_{22} - G_{12}(\Gamma^1_{12} + \Gamma^2_{22})]_{i+1,j}$$

$$DQ = [G_{22}\Gamma^2_{12} + G_{11}\Gamma^1_{22} - G_{12}(\Gamma^1_{12} + \Gamma^2_{22})]_{i-1,j}$$

$$DR = [G_{11}\Gamma^2_{12} - G_{12}\Gamma^2_{11}]_{i,j+1}$$

$$DS = [G_{11}\Gamma^2_{12} - G_{12}\Gamma^2_{11}]_{i,j-1}$$

$$DT = [G_{11}\Gamma^2_{22} - G_{12}\Gamma^2_{12}]_{i,j+1}$$

$$DU = [G_{11}\Gamma^2_{22} - G_{12}\Gamma^2_{12}]_{i,j-1}$$

With these abbreviations the finite-difference approximation of Equation (A-16) takes the following shape.

$$\begin{aligned}
\Theta_{i,j} &= (G_{12}/2\sqrt{g})_{i,j}\ (p_{i,j+1} - p_{i,j-1}) \\
&\quad - (G_{22}/2\sqrt{g})_{i,j}\ (p_{i+1,j} - p_{i-1,j}) + (p_{i,j})DA \\
&\quad + \varepsilon(G_{22}/2)_{i,j}\ [(\lambda_{k,j} + \lambda_{i+1,j})(u_{i+1,j} - u_{i,j}) \\
&\quad - (\lambda_{i,j} + \lambda_{i-1,j})(u_{i,j} - u_{i-1,j})] \\
&\quad + \varepsilon(G_{22}/4)\ [\lambda_{i+1,j}\ (v_{i+1,j+1} - v_{i+1,j-1}) \\
&\quad - \lambda_{i-1,j}(v_{i-1,j+1} - v_{i-1,j-1})] \\
&\quad + \varepsilon(G_{22}/2)\ [((\Gamma^1_{11} + \Gamma^2_{12})\ \lambda u)_{i+1,j} - ((\Gamma^1_{11} + \Gamma^2_{12})\ \lambda u)_{i-1,j}] \\
&\quad + \varepsilon(G_{22}/2)\ [((\Gamma^1_{12} + \Gamma^2_{22})\lambda v)_{i+1,j} - ((\Gamma^1_{12} + \Gamma^2_{22})\ \lambda v)_{i-1,j}] \\
&\quad - \varepsilon(G_{12}/4)\ [\lambda_{i,j+1}\ (u_{i+1,j+1} - u_{i-1,j+1}) \\
&\quad - \lambda_{i,j-1}\ (u_{i+1,j-1} - u_{i-1,j-1})] \\
&\quad - \varepsilon(G_{12}/2)\ [(\lambda_{i,j} + \lambda_{i,j+1})(v_{i,j+1} - v_{i,j}) \\
&\quad - \varepsilon(G_{12}/2)\ [((\Gamma^1_{11} + \Gamma^2_{12})\ \lambda u)_{i,j+1} - ((\Gamma^1_{11} + \Gamma^2_{12})\ \lambda u)_{i,j-1}]
\end{aligned}$$

$$- \varepsilon(G_{12}/2)\ [((\Gamma^1_{12} + \Gamma^2_{22})\lambda v)_{i,j+1} - ((\Gamma^1_{12} + \Gamma^2_{22})\lambda v)_{i,j-1}]$$

$$+ \varepsilon[((\mu G_{22})_{i,j} + (\mu G_{22})_{i+1,j})(u_{i+1,j} - u_{i,j})$$

$$- ((\mu G_{22})_{i,j} + (\mu G_{22})_{i-1,j})(u_{i,j} - u_{i-1,j})]$$

$$- (\varepsilon/2)[(\mu G_{12})_{i+1,j}\ (u_{i+1,j+1} - u_{i+1,j-1})$$

$$- (\mu G_{12})_{i-1,j}\ (u_{i-1,j+1} - u_{i-1,j-1})]$$

$$+ \varepsilon[DB(\mu u)_{i+1,j} - DC(\mu u)_{i-1,j}]$$

$$+ \varepsilon[DD(\mu v)_{i+1,j} - DE(\mu v)_{i-1,j}]$$

$$+ (\varepsilon/2)[((\mu G_{11})_{i,j} + (\mu G_{11})_{i,j+1})(u_{i,j+1} - u_{i,j})$$

$$- ((\mu G_{11})_{i,j} + (\mu G_{11})_{i,j-1})(u_{i,j} - u_{i,j-1})]$$

$$+ (\varepsilon/4)\ [(\mu G_{22})_{i,j+1}\ (v_{i+1,j+1} - v_{i-1,j+1})$$

$$- (\mu G_{22})_{i,j-1}\ (v_{i+1,j-1} - v_{i-1,j-1})]$$

$$- (\varepsilon/4)\ [\mu G_{12})_{i,j+1}\ (u_{i+1,j+1} - u_{i-1,j+1})$$

$$- (\mu G_{12})_{k,j-1}\ (u_{i+1,j-1} - u_{i-1,j-1})]$$

$$- (\varepsilon/2)\ [((\mu G_{12})_{i,j} + (\mu G_{12})_{i,j+1})(v_{i,j+1})$$

$$- ((\mu G_{12})_{i,j} + (\mu G_{12})_{i,j-1})(v_{i,j} - v_{i,j-1})]$$

$$+ (\varepsilon/2)\ [DF(\mu u)_{i,j+1} - DG(\mu u)_{i,j-1}]$$

$$+ (\varepsilon/2)\ [DH(\mu v)_{i,j+1} - DI(\mu v)_{i,j-1}!$$

$$+ \varepsilon\mu_{i,j}[(u_{i+1,j} - u_{i-1,j}) - (u_{i,j+1} - u_{i,j-1})]DB$$

$$+ \varepsilon\mu_{i,j}(v_{i+1,j} - v_{i-1,j})DD$$

$$- \varepsilon\mu_{i,j}(v_{i,j+1} - v_{i,j-1})\,[\Gamma^1_{12}G_{12} - \Gamma^1_{22}G_{11}]_{i,j}$$

$$+ 2\varepsilon(\mu u)_{i,j}\,[(\Gamma^1_{11})_{i,j}\,DB + (\Gamma^1_{12})_{i,j}\,DF + (\Gamma^1_{22})_{i,j}\,DJ]$$

$$+ 2\varepsilon(\mu v)_{i,j}\,[\Gamma^1_{11})_{i,j}\,DK + (\Gamma^1_{12})_{i,j}\,DL + (\Gamma^1_{22})_{i,j}\,DM] \qquad \text{(C-9)}$$

$$\phi_{i,j} = (G_{12}/\sqrt{g})_{i,j}\,(p_{i+1,j} - p_{i-1,j})$$

$$- (G_{11}/\sqrt{g})_{i,j}\,(p_{i,j+1} - p_{i,j-1}) + p_{i,j}\,DN$$

$$+ (\varepsilon/4)(G_{11})_{i,j}\,[\lambda_{i,j+1}\,(u_{i+1,j+1} - u_{i-1,j+1})$$

$$- \lambda_{i,j-1}\,(u_{i+1,j-1} - u_{i-1,j-1})]$$

$$+ (\varepsilon/2)(G_{11})_{i,j}\,[(\lambda_{i,j} + \lambda_{i,j+1})(v_{i,j+1} - v_{i,j})$$

$$- (\lambda_{i,j} + \lambda_{i,j-1})(v_{i,j} - v_{i,j-1})$$

$$+ ((\Gamma^1_{11} + \Gamma^2_{12})\lambda u)_{i,j+1} - ((\Gamma^1_{11} + \Gamma^2_{12})\lambda u)_{i,j-1}$$

$$+ ((\Gamma^1_{12} + \Gamma^2_{22})\lambda v)_{i,j+1} - ((\Gamma^1_{12} + \Gamma^2_{22})\lambda v)_{i,j-1}]$$

$$- (\varepsilon/2)(G_{12})_{i,j}\,[(\lambda_{i,j} + \lambda_{i+1,j})(u_{i+1,j} - u_{i,j})$$

$$- (\lambda_{i,j} + \lambda_{i-1,j})(u_{i,j} - u_{i-1,j})]$$

$$- (\varepsilon/4)(G_{12})_{i,j}\,[\lambda_{i+1,j}\,(v_{i+1,j+1} - v_{i+1,j-1})$$

$$- \lambda_{i-1,j}\,(v_{i-1,j+1} - v_{i-1,j-1})]$$

$$
\begin{aligned}
&- (\varepsilon/2)(G_{12})_{i,j}\,[((\Gamma^1_{11} + \Gamma^2_{12})\lambda u)_{i+1,j} \\
&- ((\Gamma^1_{11} + \Gamma^2_{12})\lambda u)_{i-1,j} - ((\Gamma^1_{12} + \Gamma^2_{22})\lambda v)_{i+1,j} \\
&- ((\Gamma^1_{12} + \Gamma^2_{22})\lambda v)_{i-1,j} \\
&+ (\varepsilon/4)\,[(\mu G_{11})_{i+1,j}\,(u_{i+1,j+1} - u_{i+1,j-1}) \\
&- (\mu G_{11})_{i-1,j}\,(u_{i-1,j+1} - u_{i-1,j-1})] \\
&+ (\varepsilon/2)\,[((\mu G_{22})_{i,j} + (\mu G_{22})_{i+1,j})(v_{i+1,j} - v_{i,j}) \\
&- ((\mu G_{22})_{i,j} + (\mu G_{22})_{i-1,j})(v_{i,j} - v_{i-1,j}) \\
&- ((\mu G_{12})_{i,j} + (\mu G_{12})_{i+1,j})\,(u_{i+1,j} - u_{i,j}) \\
&+ ((\mu G_{12})_{i,j} + (\mu G_{12})_{i-1,j})(u_{i,j} - u_{i-1,j})] \\
&- (\varepsilon/4)\,[(\mu G_{12})_{i+1,j}\,(v_{i+1,j+1} - v_{i+1,j-1}) \\
&- (\mu G_{12})_{i-1,j}\,(v_{i-1,j+1} - v_{i-1,j-1})] \\
&+ (\varepsilon/2)\,[(\mu u)_{i+1,j}\,DF - (\mu u)_{i-1,j}\,DO \\
&+ (\mu v)_{i+1,j}\,DP - (\mu v)_{i-1,j}\,DQ] \\
&+ \varepsilon[((\mu G_{11})_{i-j} + (\mu G_{11})_{i,j+1})(v_{i,j+1} - v_{i,j}) \\
&- ((\mu G_{11})_{i,j} + (\mu G_{11})_{i,j-1})(v_{i,j} - v_{i,j-1})] \\
&- (\varepsilon/2)[(\mu G_{12})_{i,j+1}\,(v_{i+1,j+1} - v_{i-1,j+1}) \\
&- (\mu G_{12})_{i,j-1}\,(v_{i+1,j-1} - v_{i-1,j-1})]
\end{aligned}
$$

$$+ \varepsilon[(\mu u)_{i,j+1}\,DR - (\mu u)_{i,j-1}\,DS$$

$$+ (\mu v)_{i,j+1}\,DT - (\mu v)_{i,j-1}\,DU]$$

$$+ \varepsilon\mu_{i,j}[(u_{i+1,j} - u_{i-1,j})(\Gamma^2_{11}G_{22})_{i,j} - (\Gamma^2_{12}G_{12})_{i,j})$$

$$+ (u_{i,j+1} - u_{i,j-1})DJ$$

$$+ (v_{i+1,j} - v_{i-1,j})((\Gamma^2_{12}G_{22})_{i,j} - (\Gamma^2_{22}G_{12})_{i,j})$$

$$+ (v_{i,j+1} - v_{i,j-1})((\Gamma^2_{22}G_{11})_{i,j} - (\Gamma^2_{12}G_{12})_{i,j})]$$

$$+ 2\varepsilon(\mu u)_{i,j}[(\Gamma^2_{11})_{i,j}\,DB + (\Gamma^2_{12})_{i,j}\,DF + (\Gamma^2_{22})_{i,j}\,DJ]$$

$$+ 2\varepsilon(\mu v)_{i,j}\,[(\Gamma^2_{11})_{i,j}\,DK + (\Gamma^2_{12})_{i,j}\,DL + (\Gamma^2_{22})_{i,j}\,DM] \qquad \text{(C-10)}$$

$$\Psi_{i,j} = \varepsilon[(\sqrt{g}v^1)_{i+1,j} - (\sqrt{g}v^1)_{i-1,j} + (\sqrt{g}v^2)_{i,j+1} - (\sqrt{g}v^2)_{i,j-1}]$$

$$+ (\alpha_o/2)[((\mu G_{22})_{i,j} + (\mu G_{22})_{i+1,j})(T_{i+1,j} - T_{i,j})$$

$$- ((\mu G_{22})_{i,j} + (\mu G_{22})_{i-1,j})(T_{i,j} - T_{i-1,j})]$$

$$- (\alpha_o/4)[(\mu G_{12})_{i+1,j}\,(T_{i+1,j+1} - T_{i+1,j-1})$$

$$- (\mu G_{12})_{i-1,j}\,(T_{i-1,j+1} - T_{i-1,j-1})]$$

$$+ (\alpha_o/2)[((\mu G_{11})_{i,j} + (\mu G_{11})_{i,j+1})(T_{i,j+1} - T_{i,j})$$

$$- ((\mu G_{11})_{i,j} + (\mu G_{11})_{i,j-1})(T_{i,j} - T_{i,j-1})]$$

$$- (\alpha_o/4)[(\mu G_{12})_{i,j+1}\,(T_{i+1,j+1} - T_{i-1,j+1})$$

$$- (\mu G_{12})_{i,j-1}\,(T_{i+1,j-1} - T_{i-1,j-1})] \qquad \text{(C-11)}$$

APPENDIX-D

The non-dimensionalization of the N-S Equations is given in many standard text books. The non-dimensionalization of the other equations such as the Sutherland viscosity law, the thermodynamic equations of state, etc., are given in this Appendix.

Even in the range of super-sonic Mach Numbers, $M_\infty < 6$ in air, the temperature rise in the gaseous stream is high enough to force us to take into account the effect of temperature on the properties of the gas, in particular, on its viscosity. The kinematic viscosity of most gases, and of air among them, increases considerably as the temperature is increased. The temperature dependence of viscosity $\mu(T)$ must be obtained from experiments. The Sutherland viscosity law is:

$$\mu^* = C[(T^*)^{1.5}/(T^* + S^*)] \qquad \text{(D-1)}$$

where C and S_1 are constants and for air have the values $C = 2.27 \times 10^{-8}$ and $S^* = 110°K$. Dividing Equation (D-1) by the corresponding expression for free stream conditions, we get:

$$(\mu^*/\mu^*_\infty) = (T^*/T^*_\infty)^{1.5}\ [(T^*_\infty + S^*)/(T^* + S^*)]$$

or in nondimensional terms

$$\mu = T^{1.5}\ (1 + S_1)/(T + S_1) \qquad \text{(D-2)}$$

where $S_1 = S^*/T^*_\infty$

The nondimensional equation of state is obtained as follows:

since $p^* = \rho^*(c_p - c_v)T^*$ (D-3)

$$p^*/\rho_\infty^* U_\infty^* = \rho(c_p - c_v)(T^*/U_\infty^{*2})(c_p/c_p)$$

$$= \rho(\gamma_o - 1)\, C_p T^*/(\gamma_o U_\infty^{*2})$$

$$= \rho(\gamma_o - 1)\, C_p T_\infty^* T/(\gamma_o U_\infty^{*2})$$

$$= \rho(\gamma_o - 1)\, h_\infty^* T/(\gamma_o U_\infty^{*2})$$

$$= \rho(\gamma_o - 1)\, T/(\gamma_o(\gamma_o - 1)M_\infty^2)$$

i.e., the nondimensional equation of state is:

$$p = \rho T/\gamma_o M_\infty^2 \qquad \text{(D-4)}$$

Nondimensionalization of the equation for temperature, now

$\Psi = \rho^* e^* + (1/2)\rho^* |\underset{\sim}{V}^*|^2$, thus

$$\Psi = \Psi^*/\rho_\infty^* U_\infty^{*2} + \rho[(e^*/U_\infty^{*2}) + |\underset{\sim}{V}|^2/2], \text{ or}$$

$$(\Psi/\rho) = [(c_v T^*/U_\infty^{*2}) + |\underset{\sim}{V}|^2/2]$$

$$= [(c_v T T_\infty^* c_p/c_p U_\infty^{*2}) + |\underset{\sim}{v}|^2/2]$$

$$= [(T T_\infty^* c_p/\gamma_o U_\infty^{*2}) + |\underset{\sim}{V}|^2/2]$$

$$= [(T/\gamma_o(\gamma_o - 1)M_\infty^2) + |\underset{\sim}{V}|^2/2, \text{ or}$$

$$T = \gamma_o(\gamma_o - 1)M_\infty^2[\Psi/\rho) - |V|^2/2] \qquad \text{(D-5)}$$

where $|\underset{\sim}{V}|^2 = g_{ij} V^i V^j$

and V^i are the contravariant components, u and v, of $\underset{\sim}{V}$. Thus

$$|\underset{\sim}{V}|^2 = g_{11} u^2 + 2g_{12} uv + g_{22} v^2 \qquad \text{(D-6)}$$

The local Mach Number, which was used in plotting the Mach contours, is obtained as follows:

$$M_\ell = |\underset{\sim}{V}|/a = |\underset{\sim}{V}|/\sqrt{(\gamma_o \rho/\sigma)} \quad , \text{ or}$$

$$M_\ell = M_\infty |\underset{\sim}{V}|/\sqrt{T} \qquad \text{(D-7)}$$

D-7

BIBLIOGRAPHY

1. Victoria, Keith J. and Widhopf, George F., "Numerical Solution of the Unsteady Navier-Stokes Equations in Curvilinear Coordinates," Proceedings of the 3rd International Conference on Numerical Methods in Fluid Mechanics, Vol., II, 1973.

2. Thompson, J. F., Thames, F. C., and Mastin, C. W., "Automatic Numerical Generation of Body-Fitted Curvilinear Coordinate System for Field Containing any Number of Arbitrary Two-Dimensional Bodies," Journal of Computational Physics, Vol. 15, 1974, p. 299.

3. Thames, F. C., "Numerical Solution of the Incompressible Navier-Stokes Equations about Arbitrary Two-Dimensional Bodies," Ph.D. Dissertation, Mississippi State University, 1975.

4. Peyret, R., and Viviand, H., "Computation of Viscous Compressible Flows Based on the Navier-Stokes Equations," AGARD-AG-212, 1975.

5. Tannehill, J. C., Holst, T. L., and Rakich, J. V., "Numerical Computation of Two-Dimensional Viscous Blunt Body Flows with an Impinging Shock," AIAA J., Vol. 14, No. 2, 1976, p. 204.

6. Roache, P. J., "Computational Fluid Dynamics," Hermosa Publishers, 1976.

7. Vliegenthart, A. C., "The Shuman Filtering Operation and the Numerical Computation of Shock Waves," Journal of Engineering Science, Vol. 4, 1970, p. 341.

8. Warsi, Z. U. A., and Thompson, J. F., "Machine Solutions of Partial Differential Equations in the Numerically Generated Coordinate Systems," Mississippi State University, Aerophysics and Aerospace Engineering, Rep. No. MSSU-EIRS-77-1, August 1976.

9. Thames, F. C., Thompson, J. F., and Mastin, C. W., "Numerical Solution of the Navier-Stokes Equations for Arbitrary Two-Dimensional Airfoils," Proceedings of NASA Conference on Aerodynamic Analyses Requiring Advanced Computers, Langley Research Center, NASA SP-347, 1975.

10. MacCormack, R. W., "Numerical Solution of the Interaction of a Shock Wave with a Laminar Boundary Layer," Lecture Notes in Physics," Springer-Verlag, Berlin, New York, Vol. 8, 1972, p. 151.

11. Boris, J. P., and Book, D. L., "Flux-Corrected Transport. 1. SHASTA, A Fluid Transport Algorithm that Works," Journal of Computational Physics, Vol. 11, 1973, p. 38.

12. Harten, A., and Zwas, G., "Switched Numerical Shuman Filters for Shock Calculations," Journal of Engineering Mathematics, Vol. 6, No. 2, 1972, p. 207.

13. Billig, F. S., "Shock-Wave Shapes Around Spherical and Cylinderical-Nosed Bodies," J. Spacecraft, Vol. 4.

14. Rusanov, V. V., "A Blunt Body in a Supersonic Stream," Annual Review of Fluid Mechanics, Vol. 8, 1976, p. 377.

15. Van Dyke, M. D. and Gordon, H. D., "Supersonic Flow Past a Family of Blunt Axisymmetric Bodies," NASA Tech. Rep. R-1, 1959.

16. Warsi, Z. U. A., "A Course of Lectures on the Theoretical Aspects of Laminar Viscous Incompressible Flows," Published by the Department of Aerophysics and Aerospace Engineering, Mississippi State University, October 1975.

17. Thompson, J. F., Thames, F. C., Mastin, C. W., and Shanks, S. P., "Numerical Solutions of the Unsteady Navier-Stokes Equations for Arbitrary Bodies Using Boundary-Fitted Curvilinear Coordinates," Proceedings of Arizona/AFOSR Symposium on Unsteady Aerodynamics, Univ. of Arizona, Tucson, Arizona, 1975.

18. Thompson, J. F., Thames, F. C., and Shanks, S. P., "Use of Numerically Generated Body-Fitted Coordinate Systems for Solution of the Navier-Stokes Equations," Proceedings of AIAA 2nd Computational Fluid Dynamics Conference, Hartford, Connecticut, 1975.

19. Thompson, J. F., Thames, F. C., and Mastin, C. W., "Boundary-Fitted Curvilinear Coordinate Systems for Solution of Partial Differential Equations on Fields Containing any Number of Arbitrary Two-Dimensional Bodies," NASA Contractor's Reports, NASA CR-2729, July 1977.